Army Research Laboratory
Aberdeen Proving Ground, MD 21005-5066

ARL-TR-2390 **February 2001**

A Chemically Specific Burning Rate Predictor Model for Energetic Materials

Martin S. Miller and William R. Anderson
Weapons and Materials Research Directorate, ARL

Approved for public release; distribution is unlimited.

Abstract

The application of complex networks of elementary chemical reactions to the gas phase of burning energetic materials has increased markedly over the last decade. The exquisite complexity of these gas-phase reaction networks, coupled with available high-rigor treatments of transport, is not matched by an equivalent level of sophistication in descriptions of the condensed-phase and interfacial phenomena. Owing to the vastly more complicated, many-body nature of the condensed phase, this condition is not likely to be relieved soon. In response to these difficulties, a new semi-empirical approach to burning-rate calculation has been developed and applied to frozen ozone, cyclotrimethylenetrinitramine (RDX), and nitroglycerine. The new approach hypothesizes a single overall reaction linking the unreacted material to the net products of condensed-phase decomposition and characterizes their rate of formation according to an empirically derived pyrolysis law. These condensed-phase products become the reactants for the gas phase, which are treated in full elementary-reaction detail. Using this new semi-empirical model, a methodology for computing the relative effects of several additives on the burning rate of nitroglycerine is developed and demonstrated. Hopefully this approach will enable more rapid progress in modeling multi-ingredient propellants than did previous approaches attempting to model the condensed-phase processes in detail.

Table of Contents

		Page
	List of Figures	v
	List of Tables	vii
1.	**Introduction**	1
2.	**Conceptual Framework**	3
3.	**Mathematical Framework**	5
4.	**Example: Frozen Ozone**	12
5.	**Example: RDX**	13
6.	**Example: Nitroglycerine**	18
7.	**Effect of Chemical Additives on the Burning Rate**	27
8.	**Speculations on Practical Burning-Rate Modifiers**	31
9.	**Conclusions**	32
10.	**References**	35
	Appendix: Reaction Mechanism (DB11) for Nitroglycerine	41
	Distribution List	51
	Report Documentation Page	53

INTENTIONALLY LEFT BLANK.

List of Figures

Figure		Page
1.	Demonstration of the Universality of the Pyrolysis Law for Double-Base Propellants Based on the Work of Zenin [28]	10
2.	Quality of Fit of a Pyrolysis Law to an Evaporative Regression Mechanism Calculated From a First Principles Treatment of Frozen Ozone Deflagration [21]	11
3.	Pyrolysis Law for RDX Derived From Zenin's [28] Experimental Data	11
4.	Comparison of the Burning Rates for Frozen Ozone Computed by the New Model Developed in This Report and the Previously Published First-Principles Model	13
5.	Linear Least-Squares Fit of the Specific-Heat Data of Shoemaker et al. [30] and Miller [31] for Solid RDX Over a Range of Initial Temperatures.	14
6.	Comparison of Burning Rates for RDX Computed by the New Model to Those Computed by That of Liau [15] and to Experimental Data	15
7.	Temperature Profiles for RDX at 1 atm and 293 K, as Computed by the New Model, Compared With That of Liau [15]	16
8.	Species Profiles for RDX at 1 atm and 293 K, as Computed by the Present Model (Solid Lines), Compared With That of Liau [15]	17
9.	Mechanism for Condensed-Phase Decomposition of NG Proposed by Levy [39]	21
10.	Computed NG Burning Rates at 298 K for Different Decomposition Paths Using a New Semi-Empirical Model Compared With Experimentally Measured Rates of Andreev [40, 41] and Andreev et al. [42]	22
11.	Identification of Dominant Chemical Pathways for NG at 10 atm and 298 K Using the MSM4 Product Set	23
12.	The Effect of Two Additives, NH_3 and N_2, on the Flame Structure of NG at 10 atm and 298 K Using Levy's [39] Decomposition Product Set	28

INTENTIONALLY LEFT BLANK.

List of Tables

Table		Page
1.	Liquid-Phase Reactions in Deflagrating RDX Adopted by Various Models	4
2.	Values of Condensed-Phase Parameters Used in RDX Calculations	14
3.	Values of Condensed-Phase Parameters Used in NG Calculations	19
4.	NG Condensed-Phase Decomposition Paths Considered	19
5.	Relative Sensitivity Coefficients of the Temperature Gradient at the Surface to the Most Sensitive Reactions (in Rank Order) for NG, With MSM4 Product Set at 10 atm and 298-K Initial Temperature	26
6.	Effect of Different Chemical Additives on the Burning Rate of NG at 10 atm and 298 K Assuming the Levy [39] Decomposition Product Set	30
7.	Effect of Different Chemical Additives on the Burning Rate of NG at 10 atm and 298 K Assuming the MSM4 Decomposition Product Set	30

INTENTIONALLY LEFT BLANK.

1. Introduction

The last 10 years have seen an important paradigm shift in the modeling of energetic material combustion. Models using chemically nonspecific reaction formalisms have given way to models that promise to explain the detailed chemical nature of combustion through their explicit elementary-reaction mechanisms. The seminal prototypes for the chemically nonspecific models were developed during WWII by Parr and Crawford [1] and Rice and Ginell [2]. Typically these models considered a gasification reaction at the surface of the condensed phase and a single overall reaction in the gas phase; burning rates were computed by imposing the energy and species conservation equations in each phase and at the burning surface. A conceptual review of many of these models was given by Miller [3], and a review of their application to composite propellants was provided by Ramohalli [4]. These early models elucidate the interplay between the chemical and physical phenomena that produce the observed patterns of burning rate dependence on pressure and initial temperature and provided guidance in the choice of some physical features of composite-propellant formulation, such as oxidizer particle size. By their nature, however, these models cannot give guidance for chemical formulation and the effects of chemical additives on performance. This role had to await the development of chemically specific descriptions of the combustion. Models with explicit chemical mechanisms now dominate new development activities and are the subject of this article. We will confine ourselves in this report to steady-state combustion, although some recent work [5, 6] has addressed the role of elementary reactions in ignition.

The transition from overall reactions to detailed elementary reactions in the modeling of energetic material combustion did not occur suddenly and, in fact, is not yet complete. Thus far, the use of elementary reactions has been limited to the gas phase; our fundamental understanding of the condensed phase processes is not allowing more sophistication at present. In the interim, condensed phase reactions have been treated as one or more overall reactions. Reaction mechanisms for the gas phase were first developed apart from any attempt to compute the burning rate. As early as 1965, Sotter [7] assembled a mechanism consisting of 12 species reacting by 17 reversible reactions to describe the secondary reaction zone of double-base propellants. He numerically integrated this mechanism, neglecting transport processes, and found order-of-magnitude agreement

with experimentally determined induction times for the visible flame. In the early-to-mid 1980s, Ermolin et al. [8] worked out elementary-reaction mechanisms for ammonium perchlorate and cyclotrimethylenetrinitramine (RDX) [9], guided by mass spectrometric measurements in the flames of these condensed systems.

Attempts to compute the burning rate of an energetic material using realistic chemistry probably began with the Guirao and Williams' [10] treatment of ammonium perchlorate in 1971. Though the chemical mechanism consisted of 14 species and 10 irreversible reactions, a small problem by today's standards, computational tools at that time did not permit the simultaneous solution of the kinetics and transport. A simplified simultaneous solution of kinetics and transport for a larger mechanism of 19 species and 60 reversible reactions was reported by Hatch [11] in 1986 for nitroglycerine. A significant advance in the computational tools available for work of this type occurred in 1985 with the publication and availability of the PREMIX code [12], a user-friendly, well-documented, one-dimensional (1-D), premixed, laminar flame code. This code and its later improvements provide a high level of rigor to the description of gas-phase transport, allowing for such subtle effects as thermal diffusion and multicomponent transport to be conveniently treated. Moreover, the description of thermodynamic functions, transport parameters, reactions, and reaction rates in this code is also very general, allowing a wide scope of kinetic representations and convenient updating. Melius [13] was the first to utilize the PREMIX code in a calculation of energetic-material burning rate, addressing the case of RDX. In the United States, as a result of several Office of Naval Research and U.S. Army Research Office workshops starting in about 1987, a concerted effort was directed at understanding the physics and chemistry of RDX as a prototypical system. This focus resulted in a number of further refinements of RDX modeling [14–17]. Extensions of these general methods have been made to include cyclotetramethylenetetranitramine (HMX) [18, 19] and glycidyl azide polymer (GAP) [20]. In order to study the physical aspects of three-phase combustion, Miller [21] described a detailed chemical model applied to the combustion of frozen ozone as a prototypical energetic material for which very reliable kinetic and thermophysical data exist.

This report focuses on models that compute the burning rate based on detailed elementary reaction mechanisms in the gas phase. However, it is worth mentioning a few models that are chemically specific to some degree and utilize overall reactions to describe the gas phase. An early example of this type of model comes from BenReuven et al. [22] and BenReuven [23]. Their model treated the combustion of RDX using one overall reaction in the liquid phase, evaporation as the surface-gasification mechanism, and two overall reactions in the gas phase. Another example was advanced by Bizot and Beckstead [24], who considered double-base propellant combustion using three overall reactions in the condensed phase and two overall reactions in the gas phase. A recent model attempting to simplify the very complex chemistry involved in double-base propellants is that by Song and Yang [25]. Like the Bizot and Beckstead model, Song and Yang lump species into categories such as aldehydes and oxidizers. Yet another approach in this vein was taken by Li and Williams [26], who argued for the dissociation of HONO as the rate limiting step in the primary gas-phase mechanism of RDX and then applied an asymptotic analysis to compute the burning rate based on this one reaction. The relative simplicity of these models is appealing, but it will take time to determine the extent to which generality and even understanding is sacrificed.

2. Conceptual Framework

As previously stated, our primary interest here is in that class of models which strive to describe the gas-phase reactions as true elementary reactions, the rate coefficients for which are determined from independent kinetics experiments, reaction-rate theory, or thermochemical estimation methods. This restriction narrows the number of models to only four [14, 16, 17, 21]. In this report, we will describe a fifth approach. In developing this new approach, we will apply it to RDX. It will be helpful, therefore, to review some of the details of the other RDX models [14, 16, 17] (i.e., those in our restricted subset of model types).

All three models [14, 16, 17] defer to the experimental work of Brill et al. [27] for a description of the condensed-phase reactions in RDX. Brill et al. [27] found that RDX decomposes by two competing channels, R1 and R2 (see Table 1). Unfortunately, his experiment was unable to distinguish between several possible R2 paths, R2a, R2b, and R2c. Both Prasad et al. [16]

Table 1. Liquid-Phase Reactions in Deflagrating RDX Adopted by Various Models

Reaction Number	Reaction	Heat of Reaction at 570 K[a] (kcal/mole)	Model
R1	RDX → 3 CH_2O + 3 N_2O	−47	All [14,16,17]
R2a	RDX → 3 H_2CN + 3 NO_2	179	P&S [16], D&B [17]
R2b	RDX → 3 HCN + 3 HONO	19	—
R2c	RDX → 3 HCN + 3 NO_2 + 3 H	257	—
R2d	RDX → 3 HCN + 3/2 NO + 3/2 NO_2 + 3/2 H_2O	34	L&Y [14]

[a] This is the completed surface temperature at 1 atm.

and Davidson and Beckstead [17] elected to use R2a for the second path. Liau and Yang [14] suggested and used in their model another interpretation of Brill's measurements, R2d. The table shows that the degree of endothermicity among the different R2 paths varies dramatically. Unless condensed-phase reactions are unimportant to the deflagration of RDX, one would expect such differences to have a significant effect on the computed burning rate. Because the three models being considered differ in many details other than the condensed-phase reactions just discussed and the burning rates computed by each of the models agree quite well with experimental burning rates, it is impossible to see the effects of the different liquid-phase reactions in isolation. Nonetheless, it may be significant that the amounts of RDX decomposition reported to occur in the condensed phase vary among these models from 40% [16] to 25% [17] to a "limited" amount [14].

Even though the computational power now exists to treat condensed-phase reactions, our current knowledge of these reactions (even at the level of overall descriptions, let alone an elementary-reaction description) is very limited. This uncertainty is not confined simply to the rate coefficients, but extends to the very identities of both the reactants and products involved in these reactions. We believe that these difficulties will not soon be resolved, and it is with this prospect in mind that we propose the following new and more practical approach.

A key difficulty with chemically specific models is determining the identity and information rates of mole fractions of chemical species which first emerge from the condensed phase into the gas phase. We will show that given this knowledge and a reaction mechanism for the gas phase, the burning rate can be computed. One additional requirement is an expression relating the burning rate to the surface temperature; this will be discussed in this report. Though there is speculation required in identifying the chemical species emerging from the condensed phase, it is much reduced from having to speculate on the reactions occurring in the condensed phase and the rate coefficients of those reactions. Techniques to measure or calculate those condensed-phase processes are not likely to be realized soon; thus, the semi-empirical approach described here can be thought of as a practical, interim strategy pending the development of definitive tools for investigating the condensed phase. With these enabling simplifications, the model can be readily adapted to many worthwhile purposes, including experimental testing of gas-phase reaction mechanisms, computing the burning rate of multi-ingredient propellant formulations, and predicting the effect of chemical additives on the burning rate.

3. Mathematical Framework

We consider the 1-D, steady-state deflagration of a condensed substance, which is oriented in a coordinate system moving with the linear regression velocity such that the unreacted material at an initial temperature of T_0 extends to $x = -\infty$, the regressing surface is always at $x = 0$ with temperature T_s, and the final gaseous combustion products at temperature T_f are found at $x = +\infty$. The mass conservation equation can be integrated simply to give

$$\dot{m} = \rho u = \rho_s r, \tag{1}$$

where $\dot{m}$ is the mass burning rate or mass flux, ρ and u are the mass density and mixture mass velocity at any point in the interval, respectively, ρ_s is the mass density of the unreacted material at its initial temperature, and r is the linear regression rate of the surface. The continuity equation for each chemical species i is

$$\frac{d}{dx}(\rho Y_i V_i) + \dot{m}\frac{dY_i}{dx} - \dot{\omega}_i W_i = 0. \tag{2}$$

Here Y_i is the mass fraction of the ith species, V_i is the diffusion velocity of the ith species, $\dot{\omega}_i$ is the molar production rate by reactions of the ith species per unit volume, and W_i is the molecular weight of the ith species. Finally, the equation of energy conservation for this system is

$$\frac{d}{dx}\left(\lambda\frac{dT}{dx}\right) - \dot{m}\bar{c}_p\frac{dT}{dx} - \sum_i^N \rho Y_i V_i c_{Pi} - \sum_i^N \dot{\omega}_i h_i W_i = 0, \tag{3}$$

where λ is the mixture thermal conductivity, $\bar{c}_p$ is the mixture specific heat, c_{Pi} is the specific heat of the ith specis, h_i is the enthalpy of the ith species, and N is the total number of species being considered.

These equations are to be solved in the condensed and gas phases and their solutions matched through appropriate boundary conditions at the surface. In the condensed phase, the energy boundary conditions are

$$\begin{aligned} T &= T_0 \text{ at } x = -\infty \\ T &= T_x \text{ at } x = 0, \end{aligned} \tag{4}$$

and the species boundary conditions are

$$\begin{aligned} Y_i &= Y_i^{-\infty} \text{ at } x = -\infty \\ Y_i &= Y_i^{-0} \text{ at } x = -0. \end{aligned} \tag{5}$$

In the gas phase, the energy-equation boundary conditions are

$$T = T_s \text{ at } x = +0$$

$$\frac{dT}{dx} = 0 \text{ at } x = +\infty, \tag{6}$$

and the gas-phase boundary condition on each species is

$$Y_i = Y_i^{+0} \text{ at } x = +0$$

$$\frac{dY_i}{dx} = 0 \text{ at } x = +\infty. \tag{7}$$

At the surface between these two regions, the continuity of species and energy flux is guaranteed by the following two boundary conditions. Continuity of species flux at the surface is expressed by

$$\dot{m}Y_i^{-0} + \rho_c Y_i^{-0} V_i^{-0} = \dot{m}Y_i^{+0} + \rho_g Y_i^{+0} V_i^{+0}, \tag{8}$$

where the superscripts -0 and $+0$ and subscripts c and g refer to the condensed and gas sides of the surface, respectively. Continuity of the energy flux across the surface boundary is expressed by

$$-\lambda_c \left(\frac{dT}{dx}\right)^{-0} + \dot{m}\sum_i^N Y_i^{-0} h_i^{-0} + \rho_c \sum_i^N Y_i^{-0} V_i^{-0} h_i^{-0} =$$
$$-\lambda_g \left(\frac{dT}{dx}\right)^{+0} + \dot{m}\sum_i^N Y_i^{+0} h_i^{+0} + \rho_g \sum_i^N Y_i^{+0} V_i^{+0} h_i^{+0}. \tag{9}$$

These general equations are the starting point for our simplifications. In the gas phase, these conservation equations are solved numerically using the PREMIX [12] code as a subroutine; thus, the gas phase is treated with full rigor in our model. In the condensed phase, we assume that (1) there are no in-depth chemical reactions, and (2) molecular diffusion is negligible. With these assumptions, the energy equation in the condensed phase reduces to

$$\frac{d}{dx}\left(\lambda\frac{dT}{dx}\right) - \dot{m}\frac{d}{dx}\left(\sum_i^N Y_i h_i\right) = 0. \tag{10}$$

Integrating this equation from x = −∞ to x = −0 results in

$$\lambda_c\left(\frac{dT}{dx}\right)^{-0} = \dot{m}\sum_i^N Y_i^{-0} h_i^{-0} - \dot{m}\sum_i^N Y_i^{-\infty} h_i^{-\infty}. \tag{11}$$

Substituting equation 11 and equation 8 into equation 9 yields

$$\lambda_g\left(\frac{dT}{dx}\right)^{+0} = \dot{m}\sum_i^N\left(Y_i^{-0} h_i^{+0} - Y_i^{-\infty} h_i^{-\infty}\right). \tag{12}$$

Equation 12 is the form of the energy-flux boundary condition used in the model developed in this report. Notice that one does not need to know the enthalpies of the species on the condensed phase side of the surface at T_s, only their mass fractions there. This is important since heats of desorption of the nascent gas-phase species may be difficult to estimate. We are unaware of previously published material on this form of the energy-flux boundary condition, perhaps because of the novelty of the present context of a single overall condensed-phase reaction being coupled to a full elementary-reaction description of the gas phase. This equation enables our treatment. Notice also that neither the thermal conductivity, the mass density, nor the specific heat of the condensed phase at temperatures near the surface are required; the values of all these quantities are very uncertain. Only the specific heat and mass density of the unreacted material over the range of initial temperatures are required, at least for purposes of computing the burning rate. Of course, if the temperature profile through the condensed phase is needed, then a further integration using values for these parameters over the full condensed-phase temperature range will be required.

In order to compute a burning rate, the following information must be supplied: the enthalpy and mass density of the unreacted energetic material over the range of initial temperatures, a set of products (species and mole fractions) of the condensed-phase decomposition, a rate of appearance of these decomposition products as a function of surface temperature, and an elementary reaction mechanism through which these decomposition products react in the gas phase. The condensed-phase decomposition products become the initial or nascent gas-phase reactants.

As pointed out in our conceptual framework discussion, the identities of the condensed-phase reaction products are not known completely, even for the relatively well-studied case of RDX. For most other energetic materials, the situation is worse still. The only clear constraint we have in constructing this species set is elemental balance. Therefore, from the universe of possible product sets (i.e., those leading to a balanced overall reaction), plausible products must be selected based on either experimental knowledge of these product identities and concentrations (if available) or theoretical consideration of likely reaction paths. In general, multiplicity of such plausible product sets may occur. In this case, that which best reproduces the experimental burning rate should be chosen. Or, an average of the product sets can be taken based on the assumption of equal *a priori* probabilities of occurrence. In any case, the decomposition set chosen can be improved as new experimental data or theoretical insights become available.

The final type of information required to compute a burning rate is the rate of appearance of the condensed-phase decomposition products. For this, we appeal to the very old notion of an Arrhenius-like expression [2] relating the burning rate to the surface temperature, such as

$$\dot{m} = A_s e^{-E_s/RT_s} . \tag{13}$$

Such an expression has often been termed a "pyrolysis law" in the propellant-combustion literature. There are other forms of this expression in use [28, 29], but the above form preserves the dominant functionality without additional (probably uncertain) data. In fact, Zenin [28] prefers equation 13 to represent his experimental determination of surface temperatures vs. burning rates for a range of double-base propellants. Zenin found that this form provides a universal representation for

double-base propellants of different ingredient proportions (see Figure 1). It is this universality for a given class of propellants that impels us to adopt it here as a formalism for the rate of appearance of the condensed-phase decomposition products. In the case of double-base propellants, the mechanism for surface regression is likely to be reactive in nature because of the polymeric character of the nitrocellulose molecules. Figure 2 shows that the pyrolysis law in equation 13 also proves appropriate to a purely evaporative surface regression mechanism. Here, the surface temperature for the three-phase deflagration of frozen ozone was computed based on nonequilibrium evaporation driven by heat feedback from gas-phase reactions [21]. The steady deflagration of RDX is also believed to be predominately the result of evaporation [14]. Figure 3 shows a best-fit pyrolysis law (in the least-squares sense) for RDX using the surface-temperature and burning-rate data of Zenin [28]. Again, the fit is quite reasonable.

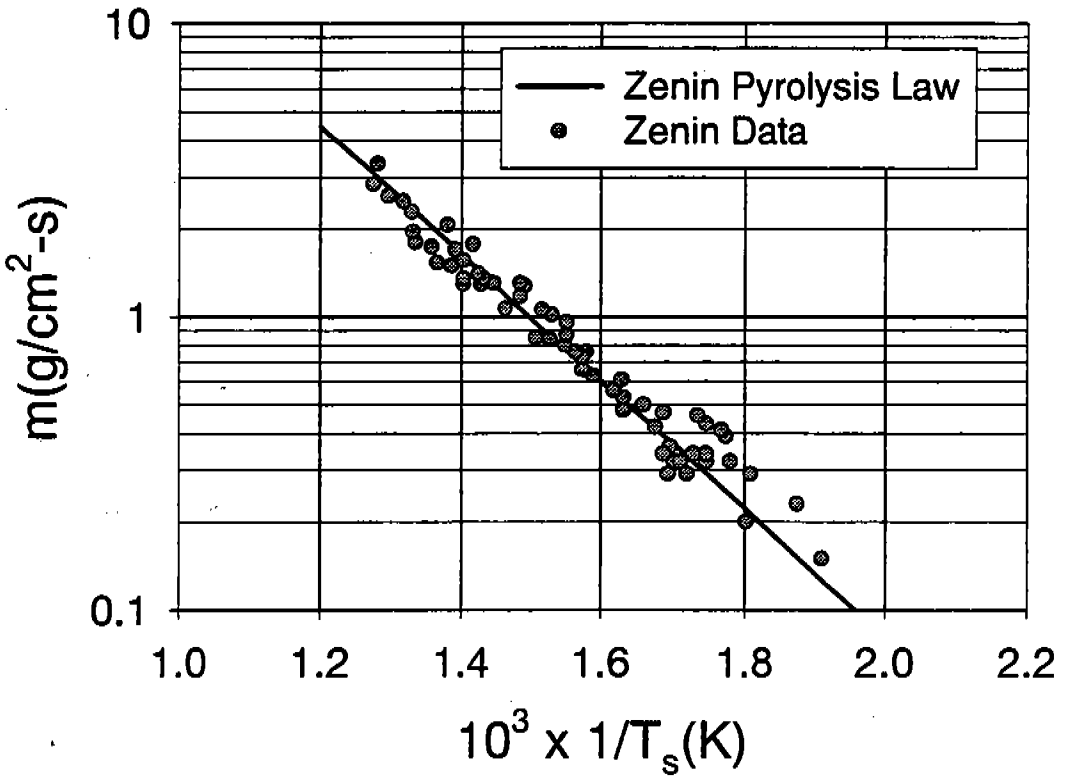

Figure 1. Demonstration of the Universality of the Pyrolysis Law for Double-Base Propellants Based on the Work of Zenin [28].

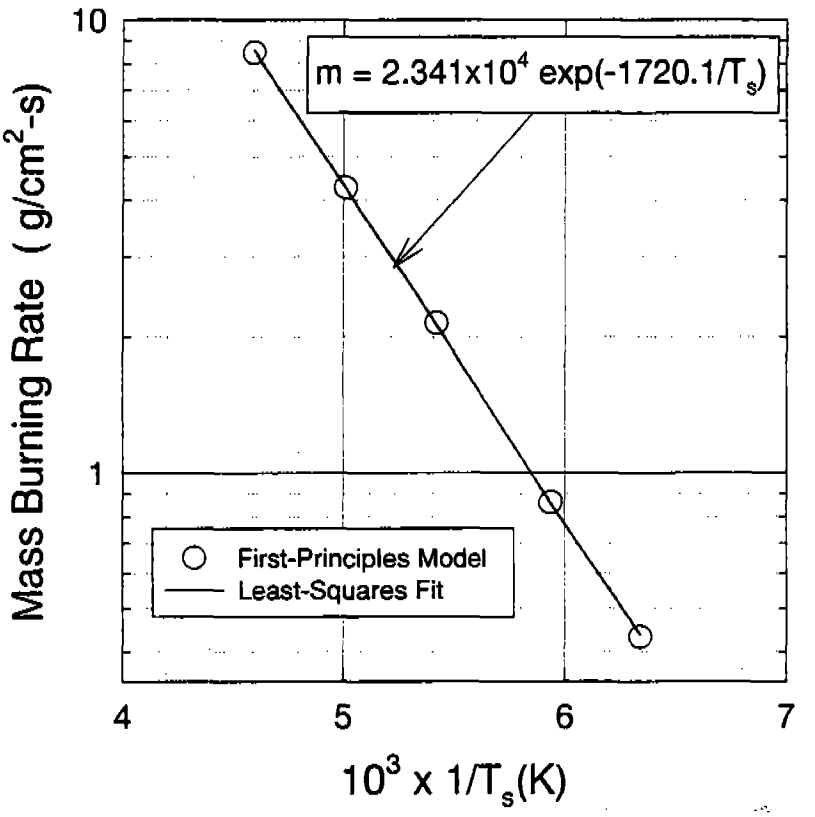

Figure 2. Quality of Fit of a Pyrolysis Law to an Evaporative Regression Mechanism Calculated From a First Principles Treatment of Frozen Ozone Deflagration [21].

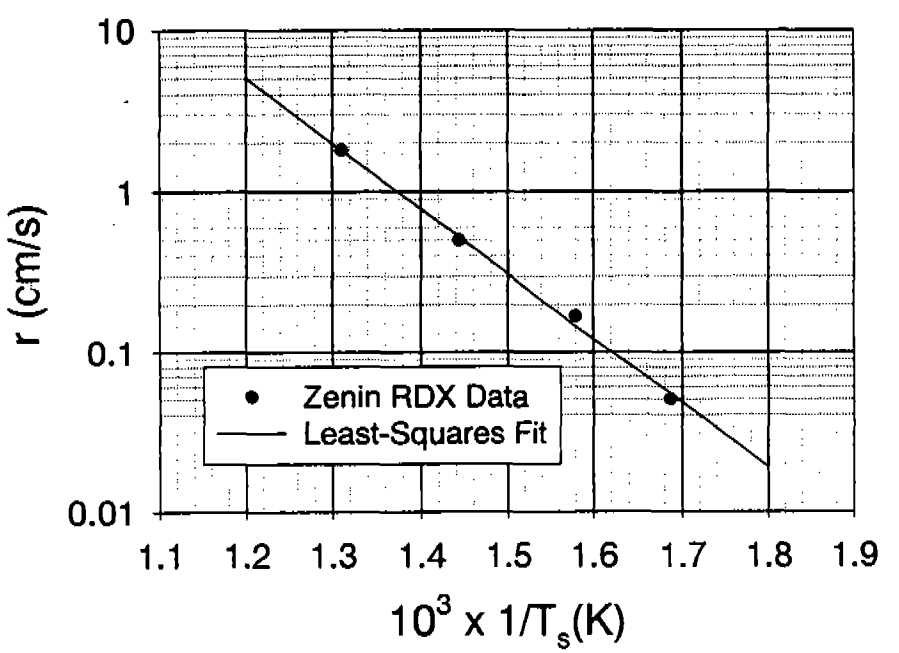

Figure 3. Pyrolysis Law for RDX Derived From Zenin's [28] Experimental Data.

4. Example: Frozen Ozone

Our first example of the application of this new model is that of the self-sustained deflagration of frozen ozone. Using the pyrolysis law previously determined from a first-principles model [21] to test for consistency, the burning rate is computed by the new model and compared with the burning rate computed by the first-principles model. Such a test is not as trivial as it might seem. The calculational details involving the evaporative surface-regression mechanism of the first-principles model is considerably more complicated than that involved in the new model. However, the evaporation process is characterized by an energy barrier (heat of vaporization), and the assumption of local thermodynamic equilibrium introduces a Boltzmann factor; this suggests that the process may be controlled by an Arrhenius-like term. On the other hand, the evaporation-mechanism equations [21] do not lead to such a simple expression, though an Arrhenius-like dependence on temperature evidently does have an implicit relevance given the excellent fit of the pyrolysis law observed in Figure 2.

Since any condensed-phase reactions in liquid ozone are too slow to influence the deflagration rate, the mechanism of surface regression is the following: evaporation driven by heat, released in gas-phase reactions, and conducted back to the surface. In this situation, the nascent gas-phase species is evaporated ozone (i.e., $Y_{O_3}^{-0} = 1$). Coupling this with the fitted pyrolysis law just described and the reaction mechanism consisting of three reversible reactions [21], we have computed the frozen ozone burning rate by our new model. It will be compared to the rate computed by the first-principles model [21]. Figure 4 shows that the agreement is excellent. The first-principles model in this case includes thermal diffusion and multicomponent transport, and the numerical grid spacing is fine enough that the burning rates are computed to an accuracy within a few tenths of a percent. Also, the central differencing option was selected. Thus, the success both of the pyrolysis law and the new model is based on a high level of computational rigor. The dominant chemical steps occurring in the gas phase for the ozone case are thoroughly discussed in Miller [21].

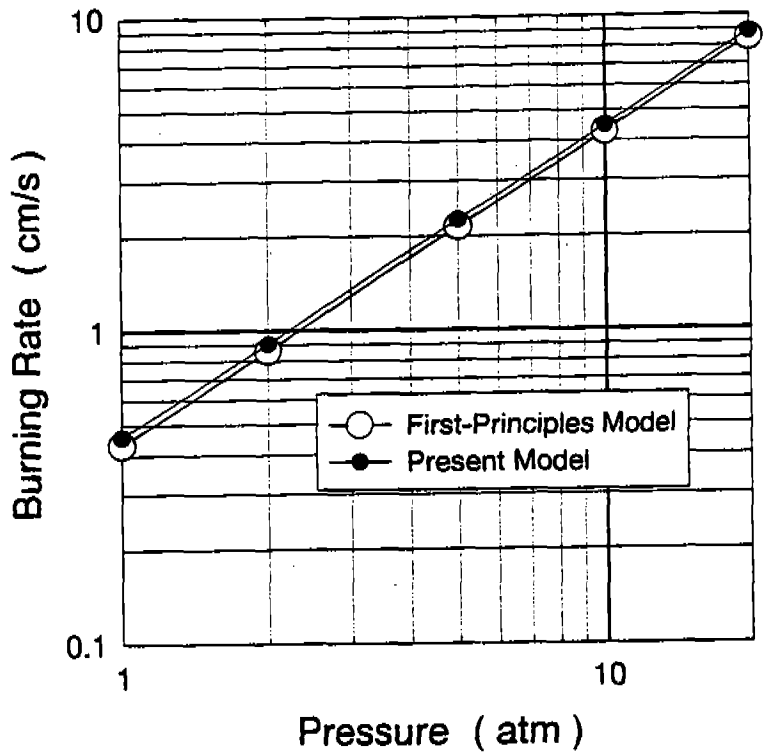

Figure 4. Comparison of the Burning Rates for Frozen Ozone Computed by the New Model Developed in This Report and the Previously Published First-Principles Model [21].

5. Example: RDX

As previously discussed, the condensed-phase decomposition paths for RDX are uncertain. Evaporation was determined to be the overwhelmingly dominant mechanism by Melius [13], Liau and Yang [14], and Liau [15], and at least predominant by Davidson and Beckstead [17] and Prasad et al. [16]. We therefore examine the consequences of assuming in our model that the surface-regression mechanism is purely evaporative. Thus, by analogy to the ozone case above, vapor-phase RDX is assumed to be the sole species emerging from the surface; mathematically this is expressed as $Y_{RDX}^{-0} = 1$. The pyrolysis law is obtained by a linearized least-squares fit to the experimental data of Zenin [28] and is illustrated in Figure 3.

The enthalpy of the solid at the initial temperature is determined as follows: the specific heat of solid RDX is obtained by a least-squares fit of a linear temperature function to the data of

Shoemaker et al. [30] and Miller [31]. The fit is shown in Figure 5 and its parameters are in Table 2. This functional form of the specific heat is integrated over temperature to determine the enthalpy of solid RDX using the value of the heat of formation at 298 K to obtain the integration constant. This treatment differs from that of Liau and Yang [14] and Liau [15], in that their model assumes a constant value of specific heat.

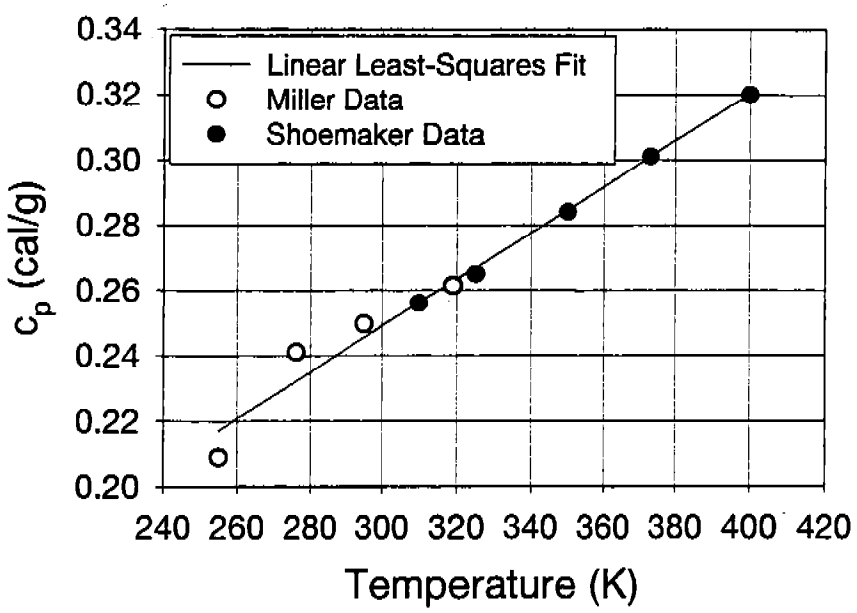

Figure 5. Linear Least-Squares Fit of the Specific-Heat Data of Shoemaker et al. [30] and Miller [31] for Solid RDX Over a Range of Initial Temperatures.

Table 2. Values of Condensed-Phase Parameters Used in RDX Calculations

Value	Description
$A_S = 6.134 \times 10^5$ g/cm^2-s	Exponential prefactor in pyrolysis law (see text)
$E_S = 18{,}539$ cal/mol	Activation energy in Pyrolysis law (see text)
$\rho_S = 1.66$ G/CM^3	Mass density of pressed solid used in experiments [28]
$W_{RDX} = 222.118$ g/mol	RDX molecular weight
$\Delta H_f^{298K} = 14{,}590$ cal/mol	RDX heat of formation at 298 K
$c_p^{solid} = 0.03604 + (7.105 \times 10^{-4})T$ cal/g-K	Specific heat of solid RDX over temperature range 260–400 K (see text)

The reaction mechanism (Yetter's second model [16]), thermodynamic data, and transport data for this case is taken from the work of Liau [15]. The burning rate (Figure 6), temperature (Figure 7), and species profiles (Figure 8) computed by the present model at an initial temperature of 293 K agrees very closely to that computed by the Liau model. (Dr. Y.-C. Liau kindly made his code available to us. All calculations in this article attributed to the Liau model [15] were made using the code version dated 13 February 1997.) We emphasize that the gas-phase reaction mechanisms, species thermodynamics, and transport parameters in both models are identical; only the treatment of the condensed phase and surface-gasification mechanism are different. The model burning rates shown in Figure 6 also compare favorably with the experimental data of Miller [32], Zenin [28], Ulas et al. [33], Homan et al. [34], and Atwood et al. [35].

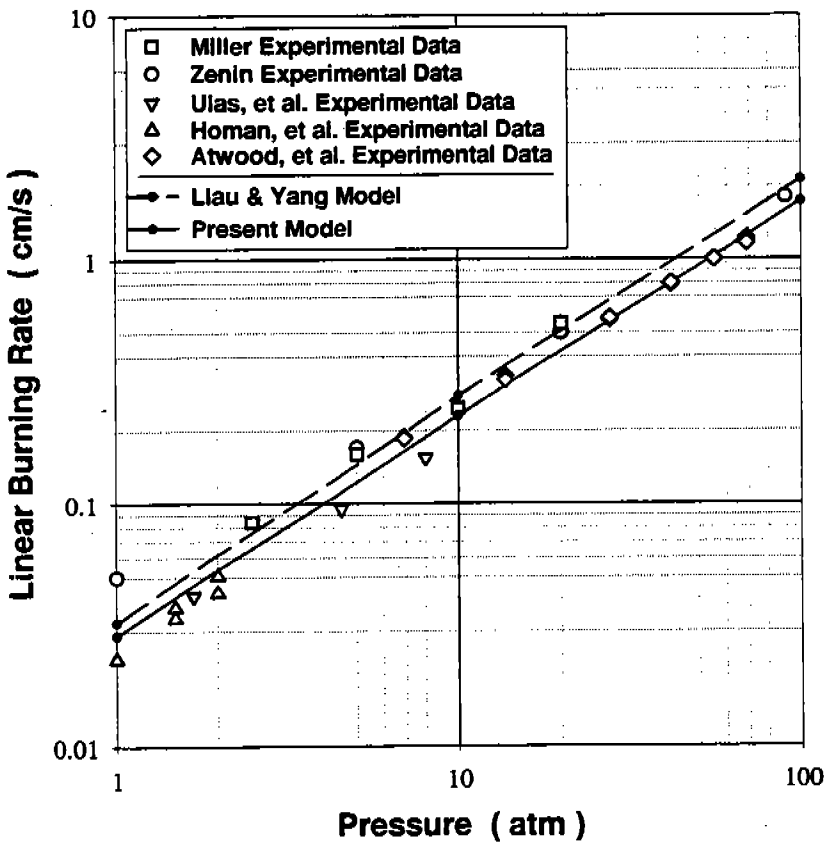

Figure 6. Comparison of Burning Rates for RDX Computed by the New Model to Those Computed by That of Liau [15] and to Experimental Data. (See Text for Experimental Data References.)

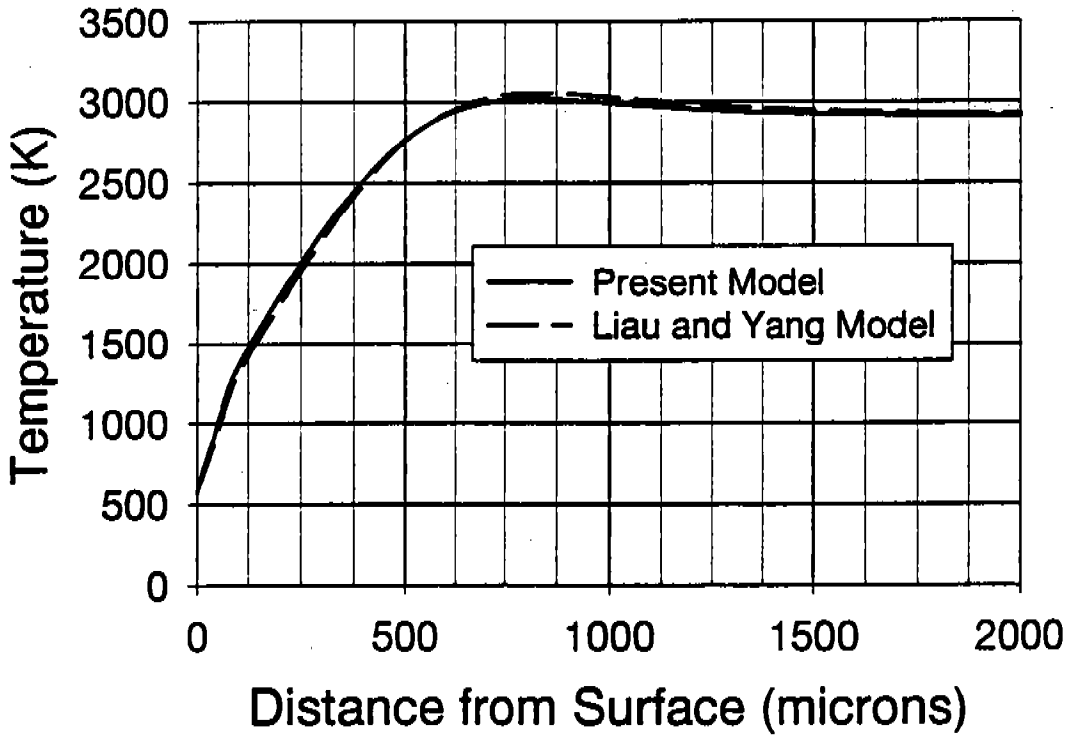

Figure 7. Temperature Profiles for RDX at 1 atm and 293 K, as Computed by the New Model, Compared With That of Liau [15].

In the RDX case, we have sought to minimize nongermane computational differences between the new semi-empirical model and that of Liau and Yang [14]. Their choice of the windward differencing option, numerical grid options, and suppression of the thermal diffusion and multicomponent transport options in PREMIX were selected for our calculations as well.

The dominant reaction paths for RDX flames have been discussed previously [13], and while the reaction mechanism has been expanded and refined since that study, we believe that the conclusions have not changed significantly. Hence, no new dominant-path analysis for RDX is given here. However, a brief explanation is now given for the slight rise in temperature above the adiabatic equilibrium value late in the flame zone, as shown in Figure 7. This behavior is surprising compared to O_2/fuel combustion in which the temperature rise is monotonic; however, it is quite typical of flames oxidized by N_2O and NO_2. In O_2 flames, there is typically an overshoot of H, O, and OH concentrations late in the flame zone, above their eventual equilibrium values. In hydrocarbon/O_2 flames, this overshoot is caused by the following radical chain-branching reactions:

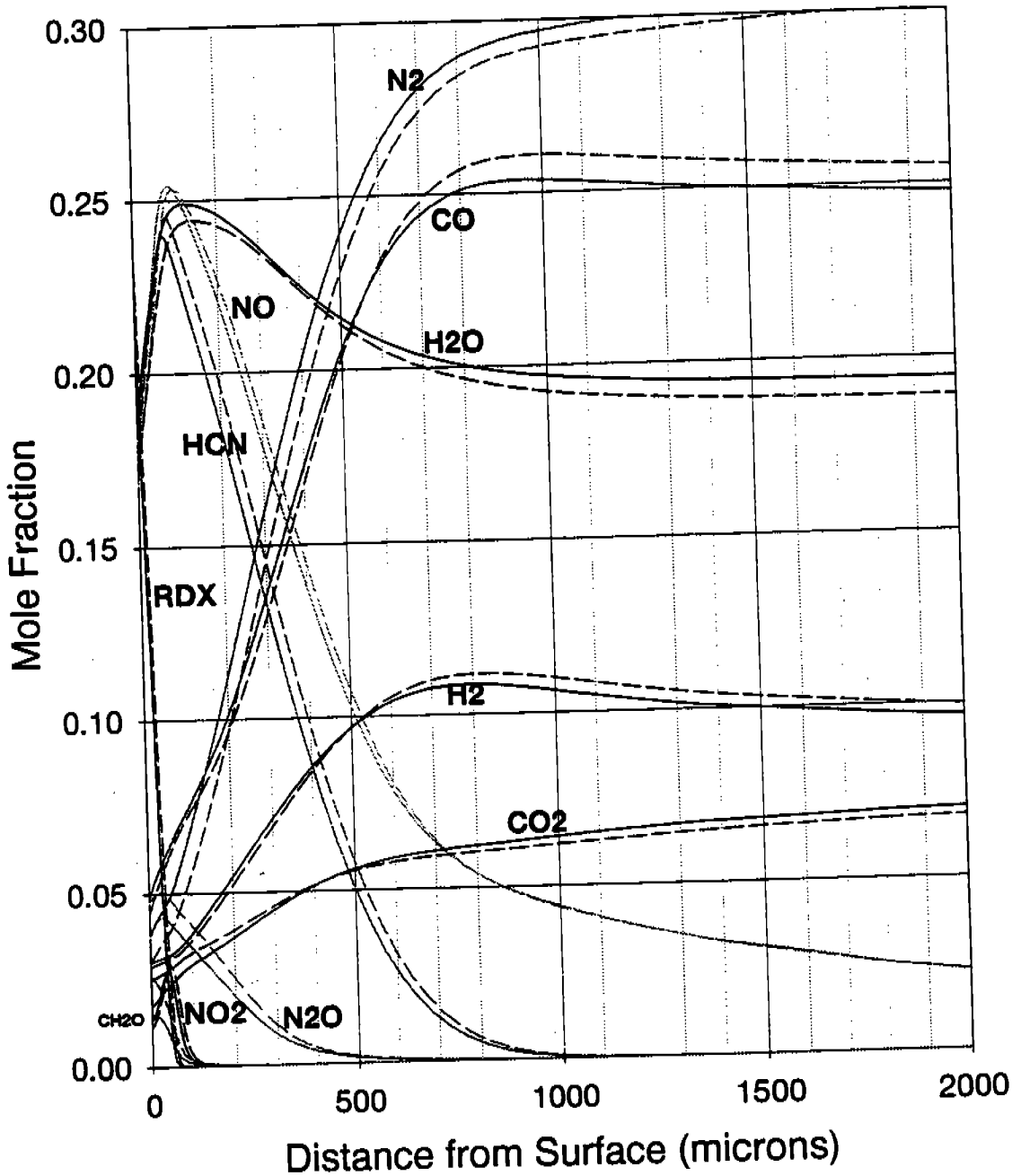

Figure 8. Species Profiles for RDX at 1 atm and 293 K, as Computed by the Present Model (Solid Lines), Compared With That of Liau [15] (Dashed Lines).

$$H + O_2 \rightarrow OH + O$$

and

$$CH_3 + O_2 \rightarrow CH_3O + O.$$

As this excess of radicals recombine in the burnt-gas region, heat is released and the temperature continues to rise to the adiabatic equilibrium value. For N_2O- and NO_2-oxidized flames, these chain branching reactions are absent. Towards the end of the flame zone, the radical concentrations are usually somewhat below their eventual equilibrium values. To reach the final equilibrium concentrations of radicals, stable species slowly decompose in the burnt gas region, absorbing heat in the process, and lowering the final temperature to the equilibrium value. For the case in Figure 7, our calculations show that H, O, and OH concentrations rise by factors of 2 to 5 between 800 and 2,000 μm. Over this same region, the temperature drops by about 100 K. A similar result was observed in computations for a low-pressure $H_2/N_2O/Ar$ flame [36].

6. Example: Nitroglycerine

Relatively little information is available on the thermal decomposition pathways of nitroglycerine (NG). We examine it here in the context of the new semi-empirical burning rate model because it represents a case of intermediate chemical complexity, it continues to play an important role in gun propellants, and it is a substance for which experimental burning rate data exists. Vital also is the fact that we could assemble a gas-phase reaction mechanism with relatively few changes from that previously developed for the dark zone of nitrate-ester and nitramine propellants [37, 38]. This was accomplished by adding only one additional species, CH_2O, and its associated reactions. The resulting mechanism (labeled DB11 here) is given in the Appendix and consists of 35 species and 178 reversible reactions. Other parameters are given in Table 3.

For the pyrolysis law, we simply use the universal double-base law determined by Zenin [28] and shown in Figure 1. Double-base propellants, of course, consist primarily of different proportions of NG and nitrocellulose. Though NG is therefore one limiting case of a double-base propellant, there is not necessarily reason to suppose the double-base pyrolysis law to be applicable to NG

Table 3. Values of Condensed-Phase Parameters Used in NG Calculations

Value	Description
$A_S = 1.8 \times 10^3$ g/cm^2-s	Exponential prefactor in pyrolysis law
$E_S = 9935$ cal/mole	Activation energy in pyrolysis law
$\rho_S = 1.59$ g/cm^3	Mass density of liquid NG
$W_{NG} = 227.087$ g/mole	NG molecular weight
$\Delta H_f^{298K} = -88{,}600$ cal/mole	NG heat of formation at 298 K
$c_p^{solid} = 0.2975$ cal/g-K	Specific heat of liquid NG

solely on this account. However, both NG and nitrocellulose are nitrate esters whose likely first step in decomposition is an NO_2 scission; if this were a rate limiting step, then the decomposition rates for NG and nitrocellulose might be expected to be similar. This argument may, in fact, be the underlying reason for the apparent universality of the double-base pyrolysis law. In any case, we will have to let the results be the ultimate justification for this assumption.

A major source of ambiguity in applying the new model to NG is the identification and quantification of the condensed-phase decomposition products, which are the nascent gas-phase species. As suggested previously, this is a situation in which a number of possibilities (consistent with a balanced reaction) must be examined and, ideally, arbitrated by broad theoretical reasoning. Again, the results must be the ultimate justification for this choice. We have examined the use of three sets of condensed-phase decomposition products for the NG case. The first is motivated by the only other elementary reaction treatment of NG of which we are aware. Hatch [11] assumed, without attempting justification, that NG decomposed by the path, as indicated in Table 4.

Table 4. NG Condensed-Phase Decomposition Paths Considered

Overall NG Decomposition Path	Reaction Path Label
NG ($C_3H_5N_3O_9$) □ 3 NO_2 + 2 CH_2O + HCO	Hatch [11]
NG □ 2 NO_2 + HONO + 2 CH_2O + CO	Levy [39]
NG □ 3 HONO + 2 HCO + CO	MSM4

We have not found a way to rationalize this path theoretically, but deem it worthwhile to consider it anyway based on its previous use. A second path, given in Table 4, was hypothesized by J. B. Levy [39] based on theoretical considerations. The steps in NG decomposition proposed by Levy are illustrated in Figure 9. A third set (MSM4) of decomposition products is also given in Table 4 and is used to compute burning rates. No theoretical justification based on a detailed sequence of paths is offered for this set, but it does lead to good agreement with experimental rates (as will be shown). One of our aims in considering a number of condensed-phase reaction paths is to gauge the sensitivity of the computed burning rate to the choice of path.

Figure 10 shows the results of the burning rate calculations using each of the above sets of condensed-phase decomposition products at an initial temperature of 298 K. The figure also shows experimental burning rates measured by Andreev [40, 41] and Andreev et al. [42]. The MSM4 decomposition product set leads to very good agreement with the experimental burning rates over a wide range of pressure. It is also of interest to note that the burning rate can vary by as much as an order of magnitude among the possible decomposition product sets that we have considered. This finding could be considerably important to tailoring the propellant burning rate for specific purposes if a way could be found to actively influence the decomposition pathways in the condensed phase.

In all of the calculations presented here involving NG (including those of the next section), the windward differencing option and suppression of the thermal diffusion and multicomponent transport options were selected. The numerical grid options were such that the burning rates presented are numerically accurate to about 2% or better.

Since this is the most extensive, detailed chemical modeling of NG combustion ever performed, a detailed analysis of the gas phase flame for one condition is presented. The case chosen is for pure NG at 10 atm at an initial temperature of 298 K, with the assumed MSM4 product set (3HONO+2HCO+CO). This is the product set which yields the best agreement between predicted burning rates and experiment (see Figure 10). Pathway diagrams, shown in Figure 11, have been constructed for this case using a postprocessor code, PREAD, written at ARL for the PREMIX code. To obtain these diagrams, the rates were first integrated over distance from the propellant surface to

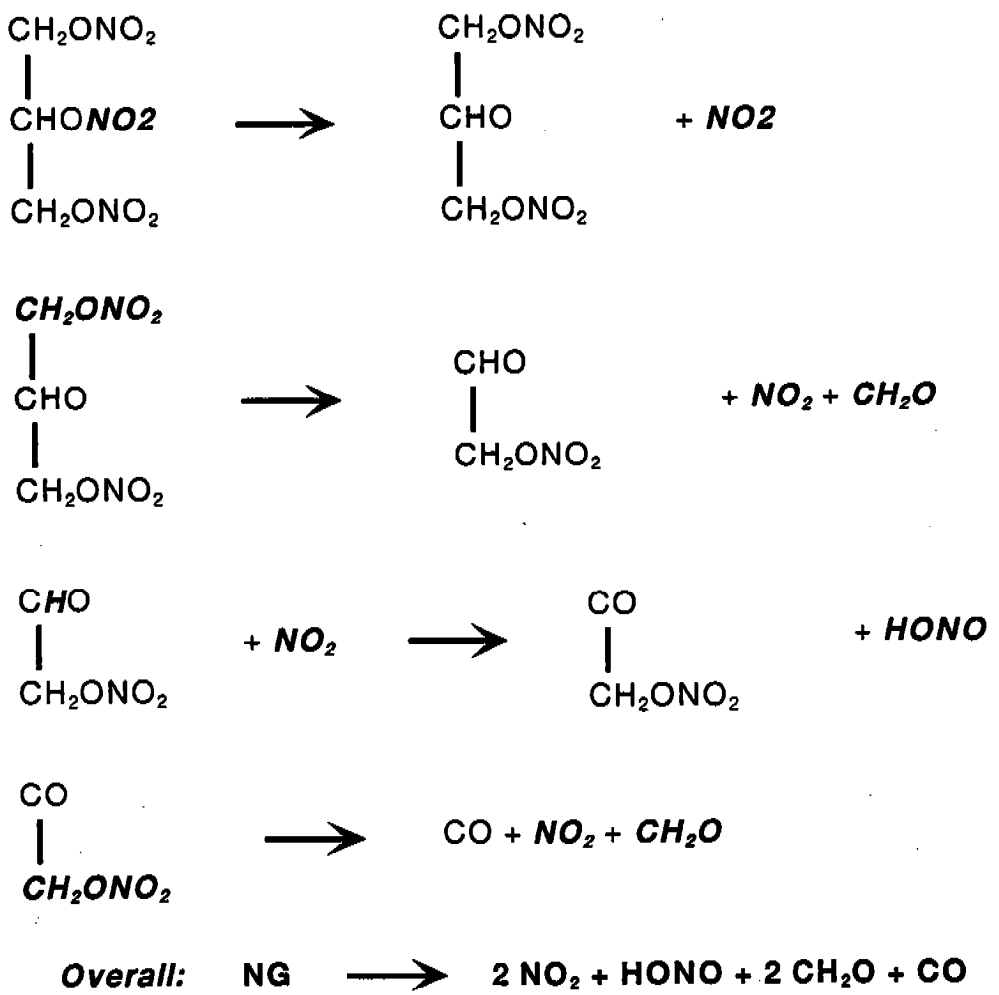

Figure 9. Mechanism for Condensed-Phase Decomposition of NG Proposed by Levy [39].

0.030 cm. This region, which we term the primary reaction zone, includes all of the near surface flame up to the leading edge of the dark zone, as determined by plateaus in temperature and key species (e.g. NO and concentration profiles [not shown]). Using the integrated rates gives a concise global picture of the chemistry in this region. The flame is quite structured in this region, however, having five separate peaks in the heat-release profile. A complete discussion of this structure is outside the scope of report, but some remarks about the structure are contained in the following discussion. The chemistry of the dark zone of NG, the region of low gradients in species concentration and temperature between the primary flame and the secondary flame (visible flame), is similar to that for double-base propellants. That case has been discussed elsewhere [37, 38].

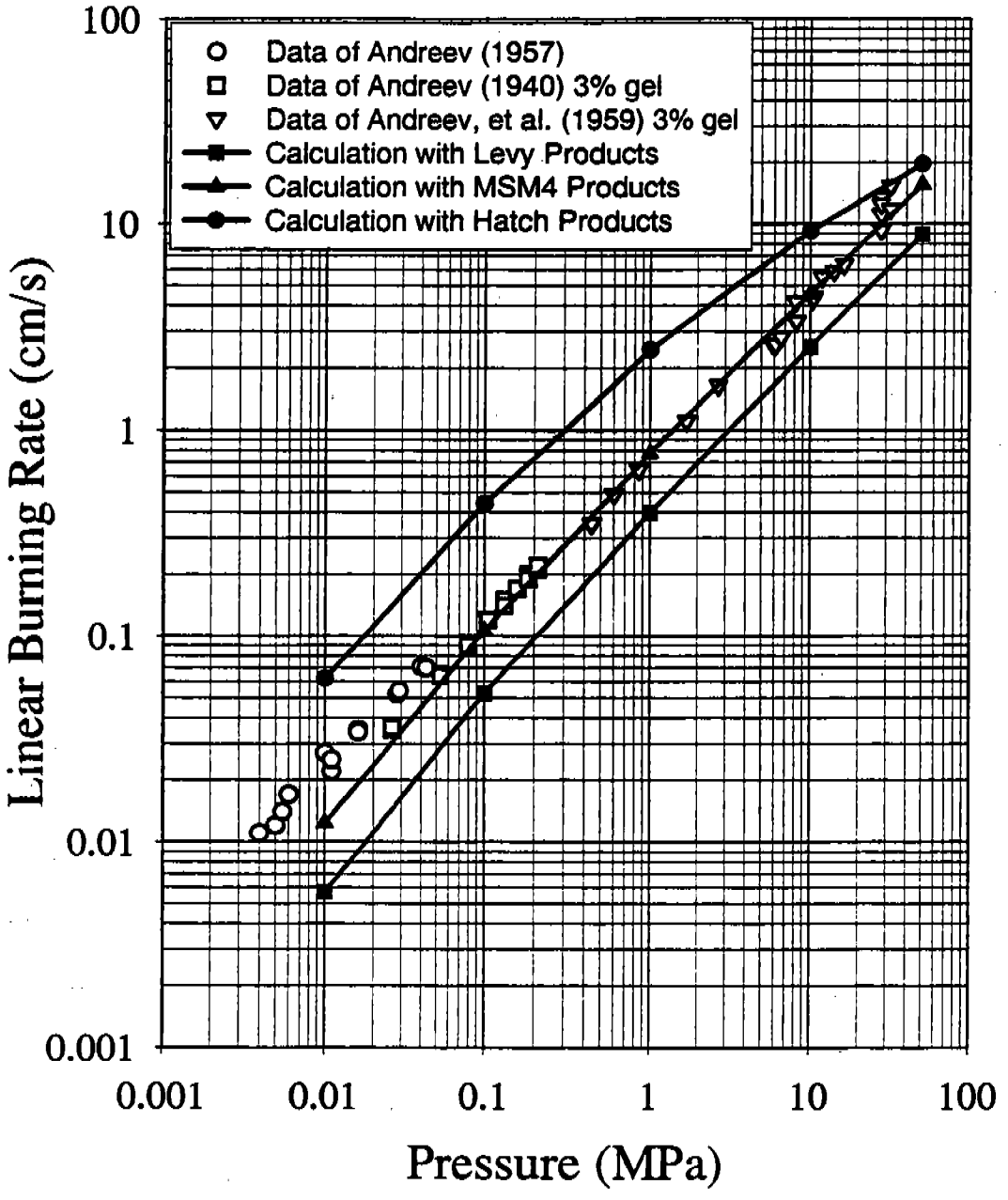

Figure 10. Computed NG Burning Rates at 298 K for Different Decomposition Paths Using a New Semi-Empirical Model Compared With Experimentally Measured Rates of Andreev [40, 41] and Andreev et al. [42].

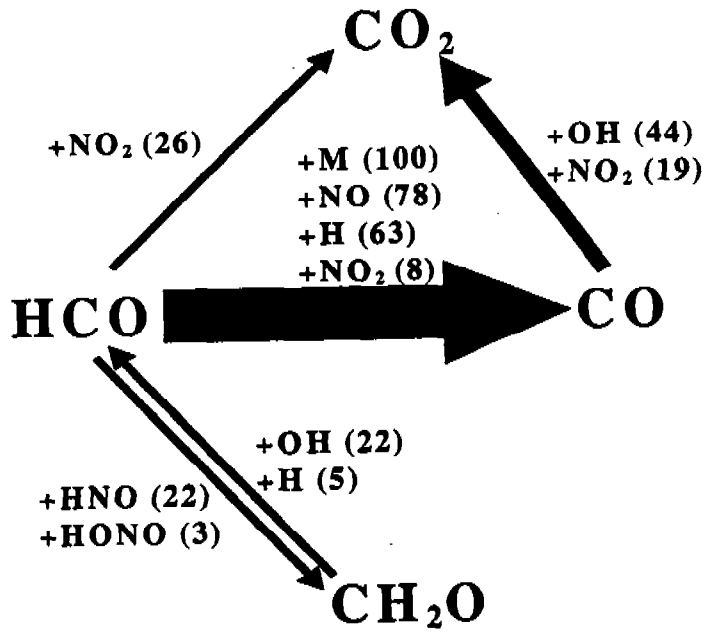

(a) Carbon-Chemistry Dominant Pathways.

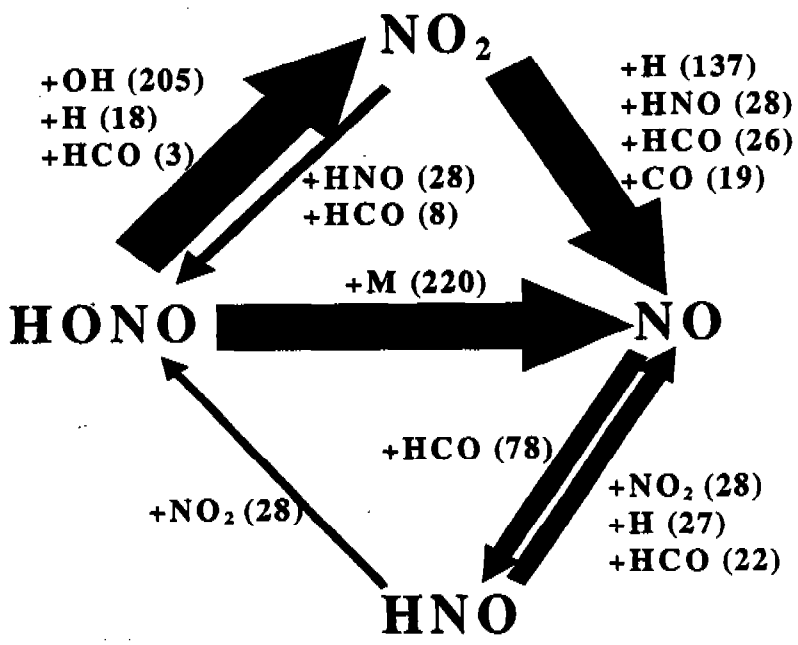

(b) Nitrogen-Chemistry Dominant Pathways.

Figure 11. Identification of Dominant Chemical Pathways for NG at 10 atm and 298 K Using the MSM4 Product Set. Numbers in Parentheses Are the Relative Rates of Each Reaction Value of 100 in Relative Units, Which Equals 8.817×10^{-3} mol/cm^2-s. Line Thickness Is Proportional to the Total, Relative, and Integrated Rates for Each Path.

The conversion of HCO to other species is very rapid, which is not surprising considering its radical nature. This conversion takes place very close to the surface, occurring within the first 0.001 cm. As shown in Figure 11a, most of the HCO is converted to CO by unimolecular decomposition or by reaction with NO, H, or NO_2. However, a portion of the HCO is temporarily converted to CH_2O, primarily by reacting with HNO. The CH_2O, being much less reactive than HCO, survives further into the primary flame. Later in the primary reaction zone, the CH_2O is converted back into HCO by reacting with OH and H; the HCO formed in this way never builds to an appreciable concentration, but is instead converted to CO or CO_2 first stage products.

The nitrogen chemistry is considered in Figure 11b. As with HCO, the conversion of HONO to other species begins rapidly near the surface because of its direct reaction with a portion of the HCO, which forms NO_2 and CH_2O. However, only a small portion of the available HONO reacts prior to the depletion of the HCO. Instead, most of the HONO conversion is delayed, occurring mainly between 0.001 and 0.015 cm. A portion of the HONO is converted directly to NO via unimolecular decomposition. However, much of it is first converted to NO_2 via reaction with OH, H, or HCO. Curiously, the conversion of NO_2 to NO takes place mainly after the burnout of the HONO. Ordinarily, in combustion involving NO_2 as a major species, it is found that NO_2 converting to NO by reacting with H atoms is so fast that it occurs at a very early point, and it controls the radical pool concentrations. But here, the HONO+M = NO+OH+M reaction is the major radical source, the HONO concentration in the region is large, and the HONO+OH rate constant is also large. This leads to HONO+M=NO+OH+M and HONO+OH = H_2O+NO_2 as the major nitrogen pathways close to the surface, rather than NO_2+H = NO+OH. The NO_2 formed early in the flame from HONO reacts higher in the flame after the HONO is gone. NO_2 is converted to NO primarily by an H atom reaction, but there are also important contributions from HNO, HCO and CO reactions. NO, the only nitrogenous species surviving into the dark zone, may be viewed as the nitrogenous "product" of the first stage combustion. The concentration of HNO is small, except very close to the surface. It appears that although their concentrations are small, HNO and NO play important roles in a catalytic cycle for the near-surface HCO conversion.

More information concerning the importance of the various reactions to the predicted burning rate may be obtained from a sensitivity analysis. The sensitivity coefficient of the temperature at a given spatial grid point to a particular reaction rate is defined as

$$S_i = \frac{A_i}{T_m}\left(\frac{\partial T}{\partial A_i}\right), \tag{14}$$

where A_i is the A-factor of the ith reaction, T is the temperature at the point of interest, and T_m is the maximum temperature observed in the entire solution. The second grid point in the solution is chosen as the point of interest because this one has special significance. The burning rate is strongly controlled by the amount of heat feedback from the gas-phase reactions to the propellant. The heat feedback rate is in turn primarily controlled by the temperature gradient at the propellant surface. Thus, the magnitude of rate constants for reactions that have a high temperature sensitivity at the second grid point in the solution must have a strong influence on the computed burning rate. In fact, to a good approximation, the sensitivity coefficient of the heat feedback is proportional to the sensitivity coefficient of the second grid point. Table 5 shows the first-order temperature sensitivities for the second gas-phase grid point of the solution (and the heat feedback) for reactions with relative values above three. For the coefficient of the second grid point, a relative value of 100 equals an absolute value of 7.769×10^{-4}. A positive temperature sensitivity coefficient indicates that an increase in the rate coefficient of the reaction will result in an increase in temperature at point two; such an increase is expected to increase the burning rate. Note that the largest sensitivity is for HCO+M = H+CO+M. This is not surprising since the reaction not only converts HCO to a final product, but produces the highly reactive H atom. Sensitivities of most of the other reactions can also be rationalized by their effects on the radical pool or formation of final products with release of heat. The only one whose high, positive sensitivity has been difficult to rationalize is the second one on the list, H_2+NO_2 = HONO+H. This reaction is reversed throughout the entire calculational domain (e.g., Figure 11b). Its reversal is not surprising since HONO is initially in the MSM4 decomposition product set. Ordinarily, since this reversed reaction converts a highly reactive H atom to comparatively unreactive species, one would expect the corresponding sensitivity would be negative. It seems likely that the explanation for the positive sensitivity is the formation of NO_2,

Table 5. Relative Sensitivity Coefficients of the Temperature Gradient at the Surface to the Most Sensitive Reactions (in Rank Order) for NG, With MSM4 Product Set at 10 atm and 298-K Initial Temperature. Positive Values Indicate Reactions That Increase the Temperature Gradient When the Rate Coefficient for the Reaction Is Increased.

Reaction Number (see Appendix)		Relative Sensitivity Coefficient
33	$HCO + M \rightleftharpoons H + CO + M$	100
139	$H_2 + NO_2 \rightleftharpoons HONO + H$	46.2
4	$NO + OH + M \rightleftharpoons HONO + M$	29.4
34	$H + HCO \rightleftharpoons H_2 + CO$	-26.4
178	$HCO + NO_2 \rightleftharpoons H + CO_2 + NO$	23.6
175	$HCO + HNO \rightleftharpoons CH_2O + NO$	21.3
177	$HCO + NO_2 \rightleftharpoons CO + HONO$	-21.3
176	$CH_2O + NO_2 \rightleftharpoons HCO + HONO$	19.6
128	$H + HNO \rightleftharpoons H_2 + NO$	-15.9
147	$HCO + NO \rightleftharpoons HNO + CO$	-4.97
157	$H + CH_2O \rightleftharpoons HCO + H_2$	-3.94
64	$NO_2 + H \rightleftharpoons NO + OH$	3.17

which in turn leads to NO and HNO formation close to the surface. The NO and HNO take part in a catalytic cycle for rapid HCO conversion to CO and CH_2O in this region (see Figure 11, both parts). This conversion occurs via reactions between HCO+NO = HNO+CO and HCO+HNO = CH_2O+NO, which release considerable heat near the surface.

Rate constants of most of the highly sensitive reactions shown in Table 5 are well established. Three exceptions are R175 (HCO+HNO=CH_2O+NO), R178 (HCO+NO_2=H+CO_2+NO), and R177 (HCO+NO_2 = CO+HONO). The rate constant expression for R175 has especially large error limits. The estimate is attributed to Tsang and Herron [43], who obtained it based on comparison to similar reactions. Rate constant expressions for R177 and R178 were obtained from Lin et al. [44]. The expressions were computed based upon *ab initio* and TST-RRKM theory. This approach should yield reasonable estimates, but experimentation is desirable.

7. Effect of Chemical Additives on the Burning Rate

It has always been hoped that theoretical modeling might some day contribute to a solution for the problem of the effects of chemical additives on the burning rate of propellants. However, only with the relatively recent advent of chemically specific modeling with elementary reactions was there any real prospect for realizing these hopes. In this section we demonstrate that theoretical guidance useful to the propellant formulator, namely the effect of additives on the burning rate, is becoming feasible.

As a first demonstration of the effects of additives on propellant flames, we took the converged values of burning rate (0.394 cm/s) and surface temperature (628 K), obtained in a calculation of NG at 10 atm using the Levy decomposition product set and the DB11 reaction mechanism, as our starting conditions for a series of steady premixed flames with several different additives. A 10% mole fraction of NH_3 was then added to the Levy product set (reducing the original product mole fractions proportionately). The flame structure was then computed and compared to the pure NG case—the result is shown in Figure 12. The two-stage flame structure is known to occur because of the reduction of HONO and NO_2 to NO in the primary reaction zone (next to the surface) and the subsequent, slower reduction of NO to N_2 in the secondary reaction zone (at the end of the dark zone). The secondary reaction zone is also known as the secondary flame or the visible flame. In that figure, the secondary gas flame for the pure NG case stands off from the surface by about a centimeter. (Notice that the distance scale is logarithmic.) This is typical of the dark zone length of double-base propellants. When the NH_3 is added, the dark zone collapses by about a factor of five. Also, the heat feedback increases by 31%. Normally, when the heat feedback increases, one can expect the burning rate to increase as well. The effect NH_3 has on the dark zone length may explain why M30 (29% nitrocellulose, 22% nitroglycerine, 47% nitroguanidine, 2% stabilizer) burns with no apparent dark zone, unlike any other gun propellant. A major ingredient in M30 is nitroguanidine, which may be expected to supply NH_2 upon decomposition. The chemical rationale for this effect will be discussed later in this report. A case with 10% N_2 added is shown in Figure 12 for comparison. The N_2 has its expected diluent effect, lowering the heat feedback by 28%, but has

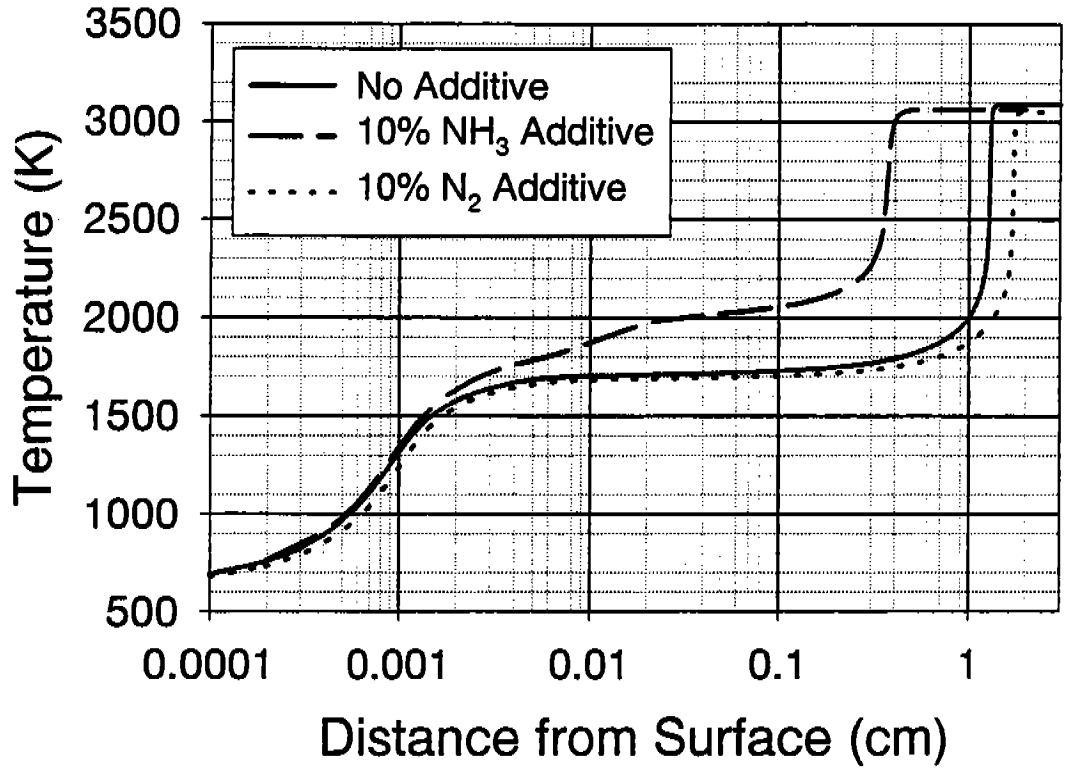

Figure 12. The Effect of Two Additives, NH_3 and N_2, on the Flame Structure of NG at 10 atm and 298 K Using Levy's [39] Decomposition Product Set. Surface Temperature and Mass Flux Are Fixed at 628 K and 0.626 g/cm^2-s, Respectively, for All Cases.

relatively little effect on the dark zone length. Liau [15] performed a similar study of the effect of various additives on the dark zone of RDX.

A more systematic approach is needed to compare the effects of one additive to another in a quantitative sense. Adopting the propellant formulation strategy of using enough additive to bring the mixture to a zero oxygen balance affords a rational method of determining the amount of each additive appropriate for comparison purposes. The oxygen balance is defined as that amount of oxygen one must add or subtract to have all oxygen appear in either H_2O or CO_2. NG has a positive balance of 3.5% (i.e., it has an oxygen surplus). Thus, we compute that one third of a mole of NH_3 must be added to effect a neutral oxygen balance for each mole of NG. For comparison, we examine two other potential additives, CH_2O and H_2. We are, of course, limited here to those fuel molecules that are already in our reaction mechanism.

Additional assumptions are required in order to model the effects of condensed-phase mixtures of ingredients. The mass density of the mixture is computed by the method of additive partial molar volumes, such as

$$\rho_{mix} = W_{avg} \Big/ \sum_i X_i V_i \,, \tag{15}$$

where W_{avg} is the average molecular weight, X_i is the mole fraction of ingredient i, and V_i is the molar volume of ingredient i. This quantity is important in calculating the linear burning rate from the mass burning rate. Secondly, we assume that the starting mixture enthalpy is given by the weighted sum of the ingredient enthalpies. This is a reasonable approximation to make, but it ignores any enthalpy of mixing or solution contributions; there is also some ambiguity as to what state is best to use for the additive enthalpy. Finally, we must, of course, assume that the pyrolysis law is unchanged as a result of these additives. This assumption is reasonable in view of the small amount of each additive.

The results of the additive computations are given in Table 6 for the Levy decomposition product set and Table 7 for the MSM4 decomposition product set. The enthalpies of all of the additives in Table 6 and Table 7 at 298 K are taken as that for the gas phase. It should be noted that this assumption could have important consequences for the computed burning rate. For example, if the enthalpy for NH_3 liquid at 298 K is used, the linear burning rate increases by only 12%. This smaller increase reflects the additional energy requirement of the heat of vaporization. Clearly, the calculation of the unreacted mixture enthalpy may require a more sophisticated theoretical treatment. In interpreting the small percentage differences shown in these tables, bear in mind that the numerical accuracy of these calculations is no worse than 2%; thus, some of the smaller effects found may not be significant.

Through sensitivity and rate analysis, we were able to identify the chemical mechanism for the burning-rate enhancement of NG by NH_3. Essentially, NH_2 reduces NO to final product N_2 by the following two most important paths,

Table 6. Effect of Different Chemical Additives on the Burning Rate of NG at 10 atm and 298 K Assuming the Levy [39] Decomposition Product Set

Additive	Weight %	Linear Burning Rate (% increase)	Mass Burning Rate (% increase)	Heat Feedback (% increase)
NH_3	2.4	19	15	19
CH_2O	3.2	1	-1	-5
H_2	0.44	1	-8	-6

Table 7. Effect of Different Chemical Additives on the Burning Rate of NG at 10 atm and 298 K Assuming the MSM4 Decomposition Product Set

Additive	Weight %	Linear Burning Rate (% increase)	Mass Burning Rate (% increase)	Heat Feedback (% increase)
NH_3	2.4	16	12	14
CH_2O	3.2	7	5	2
H_2	0.44	2	-7	-6

$$NH_2 + NO \rightarrow NNH + OH$$
$$\rightarrow N_2 + H_2O.$$

The NNH thus formed rapidly decomposes to N_2 + H. The reaction therefore leads to chain branching, which may be important to the burning rate enhancement, in addition to the increased NO conversion rate to N_2. The NH_2 is formed from NH_3, predominately by the following reaction:

$$NH_3 + OH \rightarrow NH_2 + H_2O.$$

This mechanism reinforces our speculation that M30 forms no dark zone due to the presence of an amino group on the nitroguanidine.

8. Speculations on Practical Burning-Rate Modifiers

The mechanism of NH_3 action invites a further discussion of the M30 case. With NH_3-modified NG, we found both a collapse in the dark-zone length and a significant boost in the burning rate. M30 has no dark zone, consistent with our NH_3-modified NG case, but it burns no faster than a single-base propellant and slower than a double-base propellant, a fact which appears to be inconsistent with our model calculation. This apparent inconsistency might be explained as follows. It is likely that the large percentage of nitroguanidine (NQ) present in M30 is responsible for the lack of burning-rate enhancement since it acts to lower the flame temperature of the propellant. Hence, the cooling effect might outweigh the rate acceleration effect for such major proportions of NQ. We would expect that if a small amount of NQ, say 2–5%, was added to either a single or double-base propellant, then the burning rate would be increased and the dark-zone length diminished. Of course, some of the benefit of the NH_2 from NQ could be hindered by the energy required to either break down its parent molecule or to get it into the gas phase, as could be seen in our model calculation's sensitivity to the NH_3 starting enthalpy state. Nonetheless, here is a concrete, theoretically inspired idea that could easily be tested. Thus, though the model needs to be further refined and expanded, it can already provide insights of potential worth to the propellant formulator.

The propellant formulator may find it expedient to tailor decreases in the burning rate as well as increases. For example, it has been found [45] that for layered propellants, at least a three-to-one ratio in the rates of the two layer materials must be attained in order to achieve desired performance enhancements. We have conducted preliminary calculations [46] showing HNCO as an additive that both decreases the heat feedback (and therefore presumably the burning rate) and decreases the visible flame standoff. As NH_2 proved to be the active molecule in increasing the heat feedback resulting from the addition of NH_3 to NG, NCO appears to be the active molecule for the HNCO additive. One factor leading to the reduced heat feedback may be that the radical NCO combines with NO and NO_2 near the surface to form relatively stable molecules such as N_2, N_2O, CO, and CO_2, thereby diminishing the rate of radical growth. Reduction in the visible flame standoff (dark zone length) may be due to the unimolecular decomposition in the dark zone of the N_2O which is

formed in the near surface region via the NCO reactions. This decomposition, $N_2O \rightarrow N_2 + O$, increases the radical growth rate in the dark zone, causing acceleration of the reactions leading to the visible flame. In fact, a decrease in the visible flame standoff may be a desirable effect in that it might reduce gun ignition delays, delays attributable to the slowness of the reactions leading to the substantial heat release of the visible flame [47]. Of course, to realize the benefits of these provocative ideas, much work is yet to be done both in searching for suitable active molecules and in finding practical substances that can release these active molecules. Now, the way is clear for a new and productive partnership between the theoreticians and the formulation chemists.

9. Conclusions

Models of energetic material combustion have increased enormously in their sophistication and complexity in recent years. Treatments of the gas phase involving dozens of species and hundreds of elementary reactions are now common. On the other hand, chemically specific descriptions of the condensed phase have not kept pace, largely because of the lack of definitive experiments and theory relating to the reaction paths there. All existing treatments of the condensed phase consider several overall reactions at most, and even these suffer from uncertainties in the identities and concentrations of the reactants and products. In the face of these intractabilities, we have developed a new semi-empirical model, one which requires as input a single overall reaction representing the conversion of unreacted energetic material to the nascent gas-phase species and a pyrolysis law expressing the relationship of surface temperature to burning rate. This approach, where the pyrolysis law is universal over some class of materials, makes the most sense; the existence of such a relation has been previously verified for double-base propellants. We have demonstrated that the simplest form of the pyrolysis law also well describes surface regression due to evaporative and reactive mechanisms. The capability of this model in describing the burning rate as a function of pressure and even species profiles (where available) was illustrated for frozen ozone, RDX, and nitroglycerine.

Key uncertainties in applying this model to energetic materials include the identity and concentrations of the products of the condensed-phase decomposition. By examining a number of

possible product sets, we found that the computed burning rate could vary by as much as an order of magnitude among these sets. This finding suggests that it might be possible to influence the burning rate of a material by stimulating decomposition along normally less favored paths.

One of the long-held hopes for chemically specific combustion modeling is the capability to compute the effects of chemical additives on the burning rate, in order to rationalize the performance tailoring of propellants. We believe that progress is rapidly being made towards fulfilling that promise. As a demonstration of this budding capability, we determined the relative effect of three additives on the burning rate of nitroglycerine where the amounts of each additive were computed to achieve a neutral oxygen balance for each mixture.

INTENTIONALLY LEFT BLANK.

10. References

1. Parr, R. G., and B. L. Crawford. "A Physical Theory of Burning of Double-Base Rocket Propellants." *Journal of Physical and Colloid Chemistry*, vol. 54, pp. 929–952, 1950.

2. Rice, O. K., and R. Ginell. "The Theory of the Burning of Double-Base Rocket Powders." *Journal of Physical and Colloid Chemistry*, vol. 54, pp. 885–917, 1950.

3. Miller, M. S. "In Search of an Idealized Model of Homogeneous Solid Propellant Combustion." *Combustion and Flame*, vol. 46, pp. 51–73, 1982.

4. Ramohalli, K. N. R. "Steady-State Burning of Composite Propellants Under Zero Cross-Flow Situation." *Fundamentals of Solid-Propellant Combustion*, edited by K. K. Kuo and M. Sumerfield, *Progress in Astronautics and Aeronautics Series, AIAA*, vol. 90, pp. 409–477, 1984.

5. Liau, Y. -C., and V. Yang. "A Time-Accurate Analysis of RDX Monopropellant Combustion With Detailed Chemistry." *Proceedings of the 32nd JANNAF Combustion Subcommittee and 1995 Propulsion Systems Hazards Subcommittee Meeting*, CPIA Publication 638, vol. I, pp. 57–67, 1995.

6. Liau, Y. -C., and V. Yang. "An Improved Model of Laser-Induced Ignition of RDX Monopropellant." *Proceedings of the 33rd JANNAF Combustion Meeting*, CPIA Publication 653, vol. II, pp. 529–545, 1996.

7. Sotter, J. G. "Chemical Kinetics of the Cordite Explosion Zone." *Proceedings of the 10th Symposium (International) on Combustion*, The Combustion Institute, Pittsburgh, PA, pp. 1405–1411, 1965.

8. Ermolin, N. E., O. P. Korobeinichev, A. G. Tereschenko, and V. M. Fomin. "Kinetic Calculations and Mechanism Definition for Reactions in an Ammonium Perchlorate Flame." *Fizika Goreniya i Vzryva*, vol. 18, pp. 61–70, 1982.

9. Ermolin, N. E., O. P. Korobeinichev, L. V. Kuibida, and V. M. Fomin. "Study of the Kinetics and Mechanism of Chemical Reactions in Hexogen Flames." *Fizika Goreniya i Vzryva*, vol. 22, pp. 544–553, 1986.

10. Guirao, C., and F. A. Williams. "A Model for Ammonium Perchlorate Deflagration Between 20 and 100 atm." *AIAA Journal*, vol. 9, pp. 1345–1356, 1971.

11. Hatch, R. L. "Chemical Kinetics Combustion Model of the NG/Binder System." *Proceedings of the 23rd JANNAF Combustion Meeting*, vol. I, pp. 157–165, October 1986.

12. Kee, R. J., J. F. Grcar, M. D. Smooke, and J. A. Miller. "A Fortran Program for Modeling Steady Laminar One-Dimensional Premixed Flames." Report SAND85-8240, Sandia National Laboratories, December 1985, reprinted March 1991.

13. Melius, C. F. "Thermochemical Modeling: II. Application to Ignition and Combustion of Energetic Materials." *Chemistry and Physics of Energetic Materials*, edited by S. Bulusu, NATO ASI 309, pp. 51–78, 1990.

14. Liau, Y. -C., and V. Yang. "Analysis of RDX Monopropellant Combustion With Two-Phase Subsurface Reactions." *Journal of Propulsion and Power*, vol. 11, pp. 729–739, 1995.

15. Liau, Y. -C. "A Comprehensive Analysis of RDX Propellant Combustion and Ignition With Two-Phase Subsurface Reactions." Ph.D. dissertation, Department of Mechanical Engineering, The Pennsylvania State University, University Park, PA, May 1997.

16. Prasad, K., R. A. Yetter, and M. D. Smooke. "An Eigenvalue Method for Computing the Burning Rates of RDX Propellants." *Combustion Science and Technology*, vol. 124, pp. 35–82, 1997.

17. Davidson, J. E., and M. W. Beckstead. "Improvements to Steady-State Combustion Modeling of Cyclotrimethylenetrinitramine." *Journal of Propulsion and Power*, vol. 13, pp. 375–383, 1997.

18. Davidson, J. E., and M. W. Beckstead. "A Three-Phase Model of HMX Combustion." *Proceedings of the 26th Symposium (International) on Combustion*, The Combustion Institute, Pittsburgh, PA, pp. 1989–1996, 1996.

19. Prasad, K., R. A. Yetter, and M. D. Smooke. "An Eigenvalue Method for Computing the Burning Rate of HMX Propellants." *Combustion and Flame*, vol. 115, pp. 406–416, 1998.

20. Davidson, J. E., and M. W. Beckstead. "A Mechanism and Model for GAP Combustion." *Proceedings of the 33rd JANNAF Combustion Meeting*, CPIA Publication 653, vol. II, pp. 91–100, 1996.

21. Miller, M. S. "Three-Phase Combustion Modelling: Frozen Ozone, a Prototype System." *Proceedings of the Materials Research Society Symposium: Decomposition, Combustion and Detonation Chemistry of Energetic Materials*, edited by T. B. Brill, T. P. Russell, W. C. Tao, and R. B. Wardle, Materials Research Society, Pittsburgh, PA, pp. 169–180, 1996.

22. BenReuven, M., L. H. Caveny, R. J. Vichnevetsky, and M. Summerfield. "Flame Zone and Sub-Surface Reaction Model for Deflagrating RDX." *Proceedings of the 16th Symposium (International) on Combustion*, The Combustion Institute, Pittsburgh, PA, pp. 1223–1233, 1977.

23. BenReuven, M. "Nitramine Monopropellant Deflagration and Non-Steady, Reacting Rocket Chamber Flows." Ph.D dissertation, Department of Mechanical and Aerospace Engineering, Princeton University, Princeton, NJ, January 1980.

24. Bizot, A., and M. W. Beckstead. "A Model for Double Base Propellant Combustion." *Proceedings of the 22nd Symposium (International) on Combustion*, The Combustion Institute, Pittsburgh, PA, pp. 1827–1834, 1989.

25. Song, H., and D. Yang. "Model for Predicting the Burning Rate of Double Base Propellants From Ingredients." *Proceedings of the 28th International Annual Conference of ICT*, Karlsruhe, Federal Republic of Germany, pp. 84-1–84-12, 24–27 June 1997.

26. Li, S. C., and F. A. Williams. "Nitramine Deflagration: Reduced Chemical Mechanism for Primary Flame Facilitating Simplified Asymptotic Analysis." *Journal of Propulsion and Power*, vol. 12, pp. 302–309, 1996.

27. Brill, T. B., H. Arisawa, P. J. Brush, P. E. Gongwer, and G. K. Williams. "Surface Chemistry of Burning Explosives and Propellants." *Journal of Physical Chemistry*, vol. 99, pp. 1384–1392, 1995.

28. Zenin, A. "HMX and RDX: Combustion Mechanism and Influence on Modern Double-Base Propellant Combustion." *Journal of Propulsion and Power*, vol. 11, pp. 752–758, 1995.

29. Ward, M. J., S. F. Son, and M. Q. Brewster. "Steady Deflagration of HMX With Simple Kinetics: A Gas Phase Chain Reaction Model." *Combustion and Flame*, vol. 114, pp. 556–568, 1998.

30. Shoemaker, R. L., J. A. Stark, and R. E. Taylor. "Thermophysical Properties of Propellants." *High Temperatures - High Pressures*, vol. 17, pp. 429–435, 1985.

31. Miller, M. S. "Thermophysical Properties of Cyclotrimethylenetrinitramine." *Journal of Thermophysics and Heat Transfer*, vol. 8, pp. 803–805, 1994.

32. Miller, M. S. U.S. Army Research Laboratory, Aberdeen Proving Ground, MD, unpublished data.

33. Ulas, A., Y. C. Lu, K. K. Kuo, and T. Freyman. "Measurement of Temperature and NO and OH Concentrations of Solid Propellant Flames Using Absorption Spectroscopy." *Proceedings of the 32nd JANNAF Combustion Meeting*, CPIA Publication 631, vol. I, pp. 461–469, 1995.

34. Homan, B. E., M. S. Miller, W. R. Anderson, and J. A. Vanderhoff. "Detailed Chemistry of RDX Combustion: Experiments and Models." *Proceedings of the 35th JANNAF Combustion Meeting*, Tucson, AZ, 1998, in press.

35. Atwood, A., P. O. Curran, C. F. Price, and J. Wiknich. "Burning Rate, Radiant Ignition, and Global Kinetics of Cyclotrimethylene Trinitramine (RDX)." *Proceedings of the 32nd JANNAF Combustion Meeting*, CPIA Publication 638, vol. I, pp. 149–159, 1995.

36. Sausa, R. C., W. R. Anderson, D. C. Dayton, C. M. Faust, and S. L. Howard. "Detailed Structure Study of a Low Pressure, Stoichiometric $H_2/N_2O/Ar$ Flame." *Combustion and Flame*, vol. 94, pp. 407–425, 1993.

37. Anderson, W. R., N. Ilincic, N. E. Meagher, K. Seshadri, and J. A. Vanderhoff. "Detailed and Reduced Chemical Kinetic Mechanisms for the Dark Zones of Double-Base and Nitramine Propellants in the Intermediate Temperature Regime." *Proceedings of the 32nd JANNAF Combustion Subcommittee Meeting and 1995 Propulsion Systems Hazards Subcommittee Meeting*, CPIA Publication 638, vol. I, pp. 197–114, 1995.

38. Ilincic, N., W. R. Anderson, K. Seshadri, and N. Meagher. "Simplified Chemical-Kinetic Mechanisms for Characterizing the Structure of the Dark Zones of Double-Base and Nitramine Propellants." *Proceedings of the 26th Symposium (International) on Combustion*, The Combustion Institute, Pittsburgh, PA, pp. 1997–2006, 1996.

39. Levy, J. B. Personal communication with E. Freedman. U.S. Army Research Laboratory, Aberdeen Proving Ground, MD.

40. Andreev, K. K. "Experimental Investigation on Combustion of Explosives." *Collection of Articles on Theory of Explosives*, Oborongiz, Moscow, pp. 39–65, 1940.

41. Andreev, K. K. "Thermal Decomposition and Combustion of Explosives." Gosenergoizdat, Moscow-Leningrad, 1957.

42. Andreev, K. K., A. P. Glazkova, and I. A. Tereshkin. "Investigation of Pressure, Temperature, and Density Influence on Combustion, Explosives, and Some Composites." Report of Chemical Physics Institute, Moscow, 1959–1960.

43. Tsang, W., and J. T. Herron. "Chemical-Kinetic Data Base for Propellant Combustion I Reactions Involving NO, NO_2, HNO, HNO_2, HCN, and N_2O." *Journal of Physical and Chemical Reference Data*, vol. 20, pp. 609–663, 1991.

44. Lin, C. Y., H. T. Wang, M. C. Lin, and C. F. Melius. "A Shock Tube Study of the $CH_2O + NO_2$ Reaction at High Temperatures." *International Journal of Chemical Kinetics*, vol. 22, pp. 455–482, 1990.

45. Robbins, F. W., and D. A. Worrell. "Fastcore Layered Propellant Study." *Proceedings of the 29th JANNAF Combustion Meeting*, CPIA Publication 593, vol. 1, pp. 91–98, 1992.

46. Miller, M. S., and W. R. Anderson. "Detailed Combustion Modeling as an Aid to Propellant Formulation: Two New Strategies." U.S. Army Research Laboratory Memorandum Report, 1999, in press.

47. Kooker, D. E., S. L. Howard, and L. -M. Chang. "Flamespreading in Granular Solid Propellant: Initial Results." *Proceedings of the 30th JANNAF Combustion Meeting*, CPIA Publication 606, vol. I, pp. 241–258, 1993.

INTENTIONALLY LEFT BLANK.

Appendix:

Reaction Mechanism (DB11) for Nitroglycerine

INTENTIONALLY LEFT BLANK.

CHEMKIN INTERPRETER OUTPUT: CHEMKIN-II Version 3.6 Apr. 1994
DOUBLE PRECISION

ELEMENTS CONSIDERED	ATOMIC WEIGHT
1. H	1.00797
2. C	12.0112
3. O	15.9994
4. N	14.0067

SPECIES CONSIDERED	PHASE	CHARGE	MOLECULAR WEIGHT	TEMPERATURE LOW	TEMPERATURE HIGH	ELEMENT COUNT H	C	O	N
1. H	G	0	1.00797	300.0	5000.0	1	0	0	0
2. H2	G	0	2.01594	300.0	5000.0	2	0	0	0
3. O2	G	0	31.99880	300.0	5000.0	0	0	2	0
4. H2O	G	0	18.01534	300.0	5000.0	2	0	1	0
5. CO2	G	0	44.00995	300.0	5000.0	0	1	2	0
6. CO	G	0	28.01055	300.0	5000.0	0	1	1	0
7. N2	G	0	28.01340	300.0	5000.0	0	0	0	2
8. NO2	G	0	46.00550	300.0	5000.0	0	0	2	1
9. N2O	G	0	44.01280	300.0	5000.0	0	0	1	2
10. NO	G	0	30.00610	200.0	6000.0	0	0	1	1
11. HONO	G	0	47.01347	300.0	5000.0	1	0	2	1
12. OH	G	0	17.00737	300.0	5000.0	1	0	1	0
13. O	G	0	15.99940	300.0	5000.0	0	0	1	0
14. HO2	G	0	33.00677	300.0	5000.0	1	0	2	0
15. H2O2	G	0	34.01474	300.0	5000.0	2	0	2	0
16. CH2O	G	0	30.02649	200.0	6000.0	2	1	1	0
17. CH3O	G	0	31.03446	300.0	3000.0	3	1	1	0
18. CH2OH	G	0	31.03446	250.0	4000.0	3	1	1	0
19. CH3OH	G	0	32.04243	300.0	5000.0	4	1	1	0
20. CH	G	0	13.01912	300.0	5000.0	1	1	0	0
21. C	G	0	12.01115	300.0	5000.0	0	1	0	0
22. HCO	G	0	29.01852	300.0	5000.0	1	1	1	0
23. NH3	G	0	17.03061	300.0	5000.0	3	0	0	1
24. NH2	G	0	16.02264	200.0	6000.0	2	0	0	1
25. NH	G	0	15.01467	200.0	6000.0	1	0	0	1
26. N	G	0	14.00670	300.0	5000.0	0	0	0	1
27. NNH	G	0	29.02137	250.0	4000.0	1	0	0	2
28. HNO	G	0	31.01407	200.0	6000.0	1	0	1	1
29. HOCO	G	0	45.01792	300.0	4000.0	1	1	2	0
30. HNNO	G	0	45.02077	300.0	5000.0	1	0	1	2
31. N2H2	G	0	30.02934	300.0	5000.0	2	0	0	2
32. N2H3	G	0	31.03731	300.0	5000.0	3	0	0	2
33. N2H4	G	0	32.04528	300.0	5000.0	4	0	0	2
34. NO3	G	0	62.00490	300.0	5000.0	0	0	3	1
35. NCO	G	0	42.01725	200.0	6000.0	0	1	1	1

```
                                                        (k = A T**b exp(-E/RT))
   REACTIONS CONSIDERED                                  A        b         E

 1. NO2(+M)=NO+O(+M)                                 7.600E+18   -1.27    73290.0
    Low pressure limit:  0.24700E+29 -0.33700E+01  0.74800E+05
    T&H VALUES  0.95000E+00 -0.10000E-03
       N2O              Enhanced by    1.500E+00
       H2O              Enhanced by    4.400E+00
       N2               Enhanced by    1.000E+00
       CO2              Enhanced by    2.300E+00
 2. N2O(+M)=N2+O(+M)                                 1.260E+12    0.00    62620.0
    Low pressure limit:  0.59700E+15  0.00000E+00  0.56640E+05
       N2O              Enhanced by    5.000E+00
       H2O              Enhanced by    7.500E+00
       N2               Enhanced by    1.000E+00
       CO2              Enhanced by    3.200E+00
       O2               Enhanced by    8.200E-01
 3. H+NO(+M)=HNO(+M)                                 1.520E+15   -0.41        0.0
    Low pressure limit:  0.40000E+21 -0.17500E+01  0.00000E+00
       N2O              Enhanced by    5.000E+00
       H2O              Enhanced by    5.000E+00
       N2               Enhanced by    1.000E+00
       CO2              Enhanced by    1.300E+00
 4. NO+OH(+M)=HONO(+M)                               1.988E+12   -0.05     -721.0
    Low pressure limit:  0.50800E+24 -0.25100E+01 -0.67600E+02
    T&H VALUE  0.62000E+00
       N2O              Enhanced by    5.000E+00
       H2O              Enhanced by    8.300E+00
       N2               Enhanced by    1.000E+00
       CO2              Enhanced by    1.500E+00
 5. NO+M=N+O+M                                       1.400E+15    0.00   148430.0
       N2               Enhanced by    1.000E+00
       H2               Enhanced by    2.200E+00
       H2O              Enhanced by    6.700E+00
       CO2              Enhanced by    3.000E+00
       N2O              Enhanced by    2.200E+00
 6. N2+M=N+N+M                                       3.710E+21   -1.60   225000.0
 7. N2O+N=N2+NO                                      1.000E+13    0.00    19870.0
 8. NO2+N=N2O+O                                      5.010E+12    0.00        0.0
 9. NO2+N=NO+NO                                      3.980E+12    0.00        0.0
10. NO2+NO2=NO+NO+O2                                 1.630E+12    0.00    26120.0
11. NO2+NO2=NO+NO3                                   9.640E+09    0.73    20920.0
12. NO2+NO3=NO+NO2+O2                                1.400E+11    0.00     3180.0
13. HNO+NO=N2O+OH                                    8.510E+12    0.00    29590.0
14. HNO+O2=HO2+NO                                    1.000E+13    0.00    25000.0
15. HNO+NO2=HONO+NO                                  6.000E+11    0.00     1987.0
16. HONO+O=OH+NO2                                    1.200E+13    0.00     5961.0
17. HONO+OH=H2O+NO2                                  1.270E+10    1.00      135.0
18. HONO+NH2=NO2+NH3                                 1.000E+10    1.00        0.0
19. HNO+O=OH+NO                                      3.610E+13    0.00        0.0
20. NH+O=NO+H                                        5.500E+13    0.00        0.0
21. NH+O=N+OH                                        3.720E+13    0.00        0.0
22. NH+NH=N2+H+H                                     5.100E+13    0.00        0.0
23. NH+M=N+H+M                                       2.650E+14    0.00    75510.0
24. NH2+NO=N2O+H2                                    5.000E+13    0.00    24640.0
25. CH+O2=HCO+O                                      3.300E+13    0.00        0.0
26. CH+O=CO+H                                        5.700E+13    0.00        0.0
```

```
27. CH+OH=HCO+H                                  3.000E+13    0.00        0.0
28. CH+CO2=HCO+CO                                3.400E+12    0.00      690.0
29. CH+H=C+H2                                    1.500E+14    0.00        0.0
30. C+O2=CO+O                                    2.000E+13    0.00        0.0
31. C+OH=CO+H                                    5.000E+13    0.00        0.0
32. OH+HCO<=>H2O+CO                              5.000E+13    0.00        0.0
33. HCO+M<=>H+CO+M                               1.870E+17   -1.00    17000.0
       H2                Enhanced by    2.000E+00
       H2O               Enhanced by    1.200E+01
       CO                Enhanced by    1.500E+00
       CO2               Enhanced by    2.000E+00
34. H+HCO<=>H2+CO                                7.340E+13    0.00        0.0
35. HCO+O=CO+OH                                  3.000E+13    0.00        0.0
36. HCO+O=CO2+H                                  3.000E+13    0.00        0.0
37. HCO+O2<=>HO2+CO                              7.600E+12    0.00      400.0
38. CO+O(+M)=CO2(+M)                             1.800E+10    0.00     2380.0
    Low pressure limit:  0.13500E+25 -0.27900E+01  0.41900E+04
    T&H VALUE  0.10000E+01
       H2O               Enhanced by    1.200E+01
       H2                Enhanced by    2.500E+00
       CO                Enhanced by    1.900E+00
       CO2               Enhanced by    3.800E+00
       N2O               Enhanced by    5.000E+00
39. CO+OH=CO2+H                                  1.510E+07    1.30     -758.0
40. CO+O2=CO2+O                                  2.530E+12    0.00    47688.0
41. HO2+CO=CO2+OH                                5.800E+13    0.00    22934.0
42. H2+O2=2OH                                    1.700E+13    0.00    47780.0
43. OH+H2=H2O+H                                  2.160E+08    1.50     3430.0
44. O2+H=O+OH                                    3.520E+16   -0.70    17070.0
45. O+H2=OH+H                                    5.060E+04    2.67     6290.0
46. H+O2+M=HO2+M                                 3.610E+17   -0.72        0.0
       H2O               Enhanced by    1.860E+01
       CO2               Enhanced by    4.200E+00
       H2                Enhanced by    2.900E+00
       CO                Enhanced by    2.100E+00
       N2                Enhanced by    1.300E+00
47. OH+HO2=H2O+O2                                7.500E+12    0.00        0.0
48. H+HO2=2OH                                    1.690E+14    0.00      874.0
49. O+HO2=O2+OH                                  1.400E+13    0.00     1073.0
50. 2OH=O+H2O                                    6.000E+08    1.30        0.0
51. 2H+M=H2+M                                    1.000E+18   -1.00        0.0
       H2                Enhanced by    0.000E+00
       H2O               Enhanced by    0.000E+00
       CO2               Enhanced by    0.000E+00
52. 2H+H2=2H2                                    9.200E+16   -0.60        0.0
53. 2H+H2O=H2+H2O                                6.000E+19   -1.25        0.0
54. 2H+CO2=H2+CO2                                5.490E+20   -2.00        0.0
55. H+OH+M=H2O+M                                 1.600E+22   -2.00        0.0
       H2O               Enhanced by    5.000E+00
56. H+O+M=OH+M                                   6.200E+16   -0.60        0.0
       H2O               Enhanced by    5.000E+00
57. O+O+M=O2+M                                   1.890E+13    0.00    -1788.0
58. H+HO2=H2+O2                                  6.630E+13    0.00     2126.0
59. 2HO2=H2O2+O2                                 1.800E+12    0.00        0.0
60. H2O2+M=2OH+M                                 1.300E+17    0.00    45500.0
61. H2O2+H=HO2+H2                                4.820E+13    0.00     7948.0
62. H2O2+OH=H2O+HO2                              1.750E+12    0.00      318.0
63. NO+HO2=NO2+OH                                2.110E+12    0.00     -479.0
```

64.	NO2+H=NO+OH		1.300E+14	0.00	361.0
65.	NO2+O=NO+O2		3.900E+12	0.00	-238.0
66.	NCO+H=NH+CO		5.400E+13	0.00	0.0
67.	NCO+O=NO+CO		4.520E+13	0.00	0.0
68.	NCO+N=N2+CO		2.000E+13	0.00	0.0
69.	NCO+OH=NO+CO+H		2.000E+13	0.00	7500.0
70.	NCO+M=N+CO+M		1.140E+23	-1.95	59930.0
	N2O	Enhanced by 5.000E+00			
	H2O	Enhanced by 5.000E+00			
	N2	Enhanced by 1.000E+00			
	CO2	Enhanced by 1.500E+00			
71.	NCO+NO=N2O+CO		8.800E+17	-1.78	790.0
72.	NCO+NO=CO2+N2		1.130E+18	-1.78	790.0
73.	NCO+NO2=CO2+N2O		1.950E+13	-0.26	-620.0
74.	NCO+NO2=CO+NO+NO		1.770E+12	-0.26	-620.0
75.	NH+O2=HNO+O		4.610E+05	2.00	6500.0
76.	NH+O2=NO+OH		1.280E+06	1.50	100.0
77.	NH+NO=N2O+H		3.500E+14	-0.46	16.1
78.	NH+NO=N2+OH		2.160E+13	-0.23	0.0
79.	N2O+H=N2+OH		2.530E+10	0.00	4550.0
	Declared duplicate reaction...				
80.	N2O+H=N2+OH		2.230E+14	0.00	16750.0
	Declared duplicate reaction...				
81.	NNH+O=N2O+H		1.400E+14	-0.40	477.0
82.	NNH+O=NO+NH		3.300E+14	-0.23	-1013.0
83.	N2O+O=N2+O2		3.654E+12	0.00	15900.0
84.	N2O+O=NO+NO		9.985E+13	0.00	28040.0
85.	H+HNO=NH+OH		3.000E+14	0.00	18000.0
86.	NH+OH=N+H2O		5.000E+11	0.50	2000.0
87.	NH+N=N2+H		3.000E+13	0.00	0.0
88.	N+H2=NH+H		1.600E+14	0.00	25140.0
89.	HNO+H=NH2+O		3.500E+15	-0.30	28200.0
90.	NH2+O=NH+OH		6.750E+12	0.00	0.0
91.	NH2+OH=NH+H2O		4.000E+06	2.00	1000.0
92.	NH2+H=NH+H2		4.000E+13	0.00	3650.0
93.	NH2+NH=N2H2+H		1.500E+15	-0.50	0.0
94.	NH2+N=N2+H+H		7.200E+13	0.00	0.0
95.	NH2+O2=HNO+OH		4.500E+12	0.00	25000.0
96.	NH2+NH2=N2H2+H2		5.000E+11	0.00	0.0
97.	NH2+NH2=NH+NH3		5.000E+13	0.00	10000.0
98.	NH2+NH2=N2H3+H		1.790E+13	-0.35	11320.0
99.	NH2+NH2+M=N2H4+M		2.980E+47	-9.44	9680.0
100.	NH2+NO2=N2O+H2O		2.840E+18	-2.20	0.0
101.	NH+NO2=N2O+OH		1.000E+13	0.00	0.0
102.	N2H4+H=N2H3+H2		1.000E+12	0.50	2000.0
103.	N2H4+OH=N2H3+H2O		3.000E+10	0.68	1290.0
104.	N2H4+O=N2H3+OH		2.000E+13	0.00	1000.0
105.	N2H3=N2H2+H		1.200E+13	0.00	58000.0
106.	N2H3+H=N2H2+H2		1.000E+12	0.50	2000.0
107.	N2H3+OH=N2H2+H2O		3.000E+10	0.68	1290.0
108.	N2H3+O=N2H2+OH		2.000E+13	0.00	1000.0
109.	N2H2+M=NNH+H+M		5.000E+16	0.00	50000.0
	H2O	Enhanced by 1.500E+01			
	O2	Enhanced by 2.000E+00			
	N2	Enhanced by 2.000E+00			
	H2	Enhanced by 2.000E+00			
110.	N2H2+H=NNH+H2		5.000E+13	0.00	1000.0
111.	N2H2+O=NH2+NO		1.000E+13	0.00	0.0

112.	N2H2+O=NNH+OH	2.000E+13	0.00	1000.0
113.	N2H2+OH=NNH+H2O	1.000E+13	0.00	1000.0
114.	N2H2+NH=NNH+NH2	1.000E+13	0.00	1000.0
115.	N2H2+NH2=NH3+NNH	1.000E+13	0.00	1000.0
116.	NH2+NO=NNH+OH	9.300E+11	0.00	0.0
117.	NH2+NO=N2+H2O	2.000E+20	-2.60	924.0
118.	NH3+OH=NH2+H2O	2.040E+06	2.04	566.0
119.	NH3+H=NH2+H2	5.420E+05	2.40	9917.0
120.	NH3+O=NH2+OH	9.400E+06	1.94	6460.0
121.	NH3+M=NH2+H+M	2.200E+16	0.00	93470.0
122.	NNH+NO=N2+HNO	2.000E+13	0.00	0.0
123.	NNH+H=N2+H2	1.000E+14	0.00	0.0
124.	NNH+OH=N2+H2O	5.000E+13	0.00	0.0
125.	NNH+NH2=N2+NH3	5.000E+13	0.00	0.0
126.	NNH+NH=N2+NH2	5.000E+13	0.00	0.0
127.	HNO+OH=NO+H2O	1.295E+07	1.88	-958.0
128.	H+HNO=H2+NO	4.460E+11	0.72	655.0
129.	HNO+NH2=NH3+NO	2.000E+13	0.00	1000.0
130.	N+NO=N2+O	3.270E+12	0.30	0.0
131.	O+NO=N+O2	3.800E+09	1.00	41375.0
132.	NO+H=N+OH	1.700E+14	0.00	48800.0
133.	HNO+HNO=N2O+H2O	3.630E-03	3.98	1190.0
134.	N2O+NO=N2+NO2	4.290E+13	0.00	47130.0
135.	NO+NO+NO=N2O+NO2	1.070E+10	0.00	26800.0
136.	HOCO+M=OH+CO+M	2.190E+23	-1.89	35270.0
137.	CO+NO2=NO+CO2	9.040E+13	0.00	33780.0
138.	CH+NO2=HCO+NO	1.010E+14	0.00	0.0
139.	H2+NO2=HONO+H	3.210E+12	0.00	28810.0
140.	NNH=N2+H	3.000E+08	0.00	0.0
	Declared duplicate reaction...			
141.	NNH+M=N2+H+M	1.000E+13	0.50	3060.0
	Declared duplicate reaction...			
142.	HNO+NO+NO=HNNO+NO2	1.700E+11	0.00	2100.0
143.	HNNO+NO=NNH+NO2	3.200E+12	0.00	270.0
144.	HNNO+NO=N2+HONO	2.600E+11	0.00	810.0
145.	HNNO+M=H+N2O+M	2.200E+15	0.00	21600.0
146.	HNNO+M=N2+OH+M	1.000E+15	0.00	25600.0
147.	HCO+NO=HNO+CO	7.230E+12	0.00	0.0
148.	O+CH2O<=>OH+HCO	3.900E+13	0.00	3540.0
149.	O+CH2OH<=>OH+CH2O	1.000E+13	0.00	0.0
150.	O+CH3O<=>OH+CH2O	1.000E+13	0.00	0.0
151.	O+CH3OH<=>OH+CH2OH	3.880E+05	2.50	3100.0
152.	O+CH3OH<=>OH+CH3O	1.300E+05	2.50	5000.0
153.	O2+CH2O<=>HO2+HCO	1.000E+14	0.00	40000.0
154.	H+HCO(+M)<=>CH2O(+M)	1.090E+12	0.48	-260.0

Low pressure limit: 0.13500E+25 -0.25700E+01 0.14250E+04
TROE centering: 0.78240E+00 0.27100E+03 0.27550E+04 0.65700E+04

H2	Enhanced by	2.000E+00
H2O	Enhanced by	6.000E+00
CO	Enhanced by	1.500E+00
CO2	Enhanced by	2.000E+00

155.	H+CH2O(+M)<=>CH2OH(+M)	5.400E+11	0.45	3600.0

```
     Low pressure limit:  0.12700E+33 -0.48200E+01  0.65300E+04
     TROE centering:      0.71870E+00  0.10300E+03  0.12910E+04  0.41600E+04
        H2                Enhanced by    2.000E+00
        H2O               Enhanced by    6.000E+00
        CO                Enhanced by    1.500E+00
        CO2               Enhanced by    2.000E+00
156. H+CH2O(+M)<=>CH3O(+M)                          5.400E+11    0.45     2600.0
     Low pressure limit:  0.22000E+31 -0.48000E+01  0.55600E+04
     TROE centering:      0.75800E+00  0.94000E+02  0.15550E+04  0.42000E+04
        H2                Enhanced by    2.000E+00
        H2O               Enhanced by    6.000E+00
        CO                Enhanced by    1.500E+00
        CO2               Enhanced by    2.000E+00
157. H+CH2O<=>HCO+H2                                2.300E+10    1.05     3275.0
158. H+CH2OH(+M)<=>CH3OH(+M)                        1.800E+13    0.00        0.0
     Low pressure limit:  0.30000E+32 -0.48000E+01  0.33000E+04
     TROE centering:      0.76790E+00  0.33800E+03  0.18120E+04  0.50810E+04
        H2                Enhanced by    2.000E+00
        H2O               Enhanced by    6.000E+00
        CO                Enhanced by    1.500E+00
        CO2               Enhanced by    2.000E+00
159. H+CH2OH<=>H2+CH2O                              2.000E+13    0.00        0.0
160. H+CH3O(+M)<=>CH3OH(+M)                         5.000E+13    0.00        0.0
     Low pressure limit:  0.86000E+29 -0.40000E+01  0.30250E+04
     TROE centering:      0.89020E+00  0.14400E+03  0.28380E+04  0.45569E+05
        H2                Enhanced by    2.000E+00
        H2O               Enhanced by    6.000E+00
        CO                Enhanced by    1.500E+00
        CO2               Enhanced by    2.000E+00
161. H+CH3O<=>H+CH2OH                               3.400E+06    1.60        0.0
162. H+CH3O<=>H2+CH2O                               2.000E+13    0.00        0.0
163. H+CH3OH<=>CH2OH+H2                             1.700E+07    2.10     4870.0
164. H+CH3OH<=>CH3O+H2                              4.200E+06    2.10     4870.0
165. H2+CO(+M)<=>CH2O(+M)                           4.300E+07    1.50    79600.0
     Low pressure limit:  0.50700E+28 -0.34200E+01  0.84350E+05
     TROE centering:      0.93200E+00  0.19700E+03  0.15400E+04  0.10300E+05
        H2                Enhanced by    2.000E+00
        H2O               Enhanced by    6.000E+00
        CO                Enhanced by    1.500E+00
        CO2               Enhanced by    2.000E+00
166. OH+CH2O<=>HCO+H2O                              3.430E+09    1.18     -447.0
167. OH+CH2OH<=>H2O+CH2O                            5.000E+12    0.00        0.0
168. OH+CH3O<=>H2O+CH2O                             5.000E+12    0.00        0.0
169. OH+CH3OH<=>CH2OH+H2O                           1.440E+06    2.00     -840.0
170. OH+CH3OH<=>CH3O+H2O                            6.300E+06    2.00     1500.0
171. HO2+CH2O<=>HCO+H2O2                            1.000E+12    0.00     8000.0
172. CH+H2O<=>H+CH2O                                1.713E+13    0.00     -755.0
173. CH2OH+O2<=>HO2+CH2O                            1.800E+13    0.00      900.0
174. CH3O+O2<=>HO2+CH2O                             4.280E-13    7.60    -3530.0
175. HCO+HNO=CH2O+NO                                6.000E+11    0.00     2000.0
176. CH2O+NO2=HCO+HONO                              8.020E+02    2.77    13730.0
177. HCO+NO2=CO+HONO                                1.240E+23   -3.29     2355.0
178. HCO+NO2=H+CO2+NO                               8.390E+15   -0.75     1930.0
```

Note: Units for the rate parameters are centimeter, second, and mole, and for E, cal/mole. For reactions followed by three numerical parameters, the rate-coefficient expression is $k = AT^b\exp(-E/RT)$. For reactions which appear twice with the phrase "declared duplicate reaction ...," the rate coefficient is computed as the sum of the two three-parameter expressions. For reactions involving a generalized collider species, M, collider efficiencies other than 1.0 are specified. For reactions involving pressure-dependent rate expressions (those with a collider species specified as [+M]), three types of expression are used. If "T&H VALUE" occurs in the output, the Tsang and Herron form was used (as described in Tsang and Herron*[1]), with constants a_0 and a_1 (if the latter is used) appearing, respectively, on the same line. A version of CHEMKIN, modified at ARL, was used for this computation. If "TROE centering:" occurs, the TROE form was used with the appropriate parameters specified on that line. If neither of these is mentioned, the Lindemann form was assumed. Descriptions of the TROE and Lindemann expressions may be found in the CHEMKIN manual.[2]

---

* Note that the log expressions used in this source are for base 10 (W. Tsang, private communication).

[1] Tsang, W., and J. T. Herron. "Chemical Kinetic Data Base for Propellant Combustion I Reactions Involving NO, NO_2, HNO, HNO_2, HCN, and N_2O." *Journal of Physical and Chemical Reference Data*, vol. 20, p. 609–663, 1991.

[2] Kee, R. J., F. M. Rupley, and J. A. Miller. "Chemkin-II: A Fortran Chemical Kinetics Package for the Analysis of Gas-Phase Chemical Kinetics." Sandia National Laboratories Report SAND89-8009, September 1989.

INTENTIONALLY LEFT BLANK.

NO. OF COPIES	ORGANIZATION
2	DEFENSE TECHNICAL INFORMATION CENTER DTIC DDA 8725 JOHN J KINGMAN RD STE 0944 FT BELVOIR VA 22060-6218
1	HQDA DAMO FDT 400 ARMY PENTAGON WASHINGTON DC 20310-0460
1	OSD OUSD(A&T)/ODDDR&E(R) R J TREW THE PENTAGON WASHINGTON DC 20301-7100
1	DPTY CG FOR RDA US ARMY MATERIEL CMD AMCRDA 5001 EISENHOWER AVE ALEXANDRIA VA 22333-0001
1	INST FOR ADVNCD TCHNLGY THE UNIV OF TEXAS AT AUSTIN PO BOX 202797 AUSTIN TX 78720-2797
1	DARPA B KASPAR 3701 N FAIRFAX DR ARLINGTON VA 22203-1714
1	US MILITARY ACADEMY MATH SCI CTR OF EXCELLENCE MADN MATH MAJ HUBER THAYER HALL WEST POINT NY 10996-1786
1	DIRECTOR US ARMY RESEARCH LAB AMSRL D D R SMITH 2800 POWDER MILL RD ADELPHI MD 20783-1197

NO. OF COPIES	ORGANIZATION
1	DIRECTOR US ARMY RESEARCH LAB AMSRL DD 2800 POWDER MILL RD ADELPHI MD 20783-1197
1	DIRECTOR US ARMY RESEARCH LAB AMSRL CI AI R (RECORDS MGMT) 2800 POWDER MILL RD ADELPHI MD 20783-1145
3	DIRECTOR US ARMY RESEARCH LAB AMSRL CI LL 2800 POWDER MILL RD ADELPHI MD 20783-1145
1	DIRECTOR US ARMY RESEARCH LAB AMSRL CI AP 2800 POWDER MILL RD ADELPHI MD 20783-1197
	ABERDEEN PROVING GROUND
4	DIR USARL AMSRL CI LP (BLDG 305)

NO. OF COPIES	ORGANIZATION
	ABERDEEN PROVING GROUND
20	DIR USARL AMSRL WM BD B E FORCH W R ANDERSON S W BUNTE C F CHABALOWSKI A COHEN R DANIEL D DEVYNCK R A FIFER B E HOMAN A J KOTLAR K L MCNESBY M MCQUAID M S MILLER A W MIZIOLEK J B MORRIS R A PESCE-RODRIGUEZ B M RICE R C SAUSA M A SCHROEDER J A VANDERHOFF

REPORT DOCUMENTATION PAGE

Form Approved
OMB No. 0704-0188

Public reporting burden for this collection of information is estimated to average 1 hour per response, including the time for reviewing instructions, searching existing data sources, gathering and maintaining the data needed, and completing and reviewing the collection of information. Send comments regarding this burden estimate or any other aspect of this collection of information, including suggestions for reducing this burden, to Washington Headquarters Services, Directorate for Information Operations and Reports, 1215 Jefferson Davis Highway, Suite 1204, Arlington, VA 22202-4302, and to the Office of Management and Budget, Paperwork Reduction Project(0704-0188), Washington, DC 20503.

1. AGENCY USE ONLY *(Leave blank)*	2. REPORT DATE	3. REPORT TYPE AND DATES COVERED
	February 2001	Final, Jan 97 - Jan 00

4. TITLE AND SUBTITLE

A Chemically Specific Burning Rate Predictor Model for Energetic Materials

5. FUNDING NUMBERS

611102AH43

6. AUTHOR(S)

Martin S. Miller and William R. Anderson

7. PERFORMING ORGANIZATION NAME(S) AND ADDRESS(ES)

U.S. Army Research Laboratory
ATTN: AMSRL-WM-BD
Aberdeen Proving Ground, MD 21005-5066

8. PERFORMING ORGANIZATION REPORT NUMBER

ARL-TR-2390

9. SPONSORING/MONITORING AGENCY NAMES(S) AND ADDRESS(ES)

10. SPONSORING/MONITORING AGENCY REPORT NUMBER

11. SUPPLEMENTARY NOTES

12a. DISTRIBUTION/AVAILABILITY STATEMENT

Approved for public release; distribution is unlimited.

12b. DISTRIBUTION CODE

13. ABSTRACT *(Maximum 200 words)*

The application of complex networks of elementary chemical reactions to the gas phase of burning energetic materials has increased markedly over the last decade. The exquisite complexity of these gas-phase reaction networks, coupled with available high-rigor treatments of transport, is not matched by an equivalent level of sophistication in descriptions of the condensed-phase and interfacial phenomena. Owing to the vastly more complicated, many-body nature of the condensed phase, this condition is not likely to be relieved soon. In response to these difficulties, a new semi-empirical approach to burning-rate calculation has been developed and applied to frozen ozone, cyclotrimethylenetrinitramine (RDX), and nitroglycerine. The new approach hypothesizes a single overall reaction linking the unreacted material to the net products of condensed-phase decomposition and characterizes their rate of formation according to an empirically derived pyrolysis law. These condensed-phase products become the reactants for the gas phase, which are treated in full elementary-reaction detail. Using this new semi-empirical model, a methodology for computing the relative effects of several additives on the burning rate of nitroglycerine is developed and demonstrated. Hopefully this approach will enable more rapid progress in modeling multi-ingredient propellants than did previous approaches attempting to model the condensed-phase processes in detail.

14. SUBJECT TERMS

modeling, energetic materials, propellant, combustion

15. NUMBER OF PAGES

49

16. PRICE CODE

17. SECURITY CLASSIFICATION OF REPORT	18. SECURITY CLASSIFICATION OF THIS PAGE	19. SECURITY CLASSIFICATION OF ABSTRACT	20. LIMITATION OF ABSTRACT
UNCLASSIFIED	UNCLASSIFIED	UNCLASSIFIED	UL

NSN 7540-01-280-5500

Standard Form 298 (Rev. 2-89)
Prescribed by ANSI Std. 239-18 298-102

INTENTIONALLY LEFT BLANK.

USER EVALUATION SHEET/CHANGE OF ADDRESS

This Laboratory undertakes a continuing effort to improve the quality of the reports it publishes. Your comments/answers to the items/questions below will aid us in our efforts.

1. ARL Report Number/Author ARL-TR-2390 (Miller) Date of Report February 2001

2. Date Report Received _____

3. Does this report satisfy a need? (Comment on purpose, related project, or other area of interest for which the report will be used.) _____

4. Specifically, how is the report being used? (Information source, design data, procedure, source of ideas, etc.) _____

5. Has the information in this report led to any quantitative savings as far as man-hours or dollars saved, operating costs avoided, or efficiencies achieved, etc? If so, please elaborate. _____

6. General Comments. What do you think should be changed to improve future reports? (Indicate changes to organization, technical content, format, etc.) _____

CURRENT ADDRESS

Organization

Name E-mail Name

Street or P.O. Box No.

City, State, Zip Code

7. If indicating a Change of Address or Address Correction, please provide the Current or Correct address above and the Old or Incorrect address below.

OLD ADDRESS

Organization

Name

Street or P.O. Box No.

City, State, Zip Code

(Remove this sheet, fold as indicated, tape closed, and mail.)

(DO NOT STAPLE)

DEPARTMENT OF THE ARMY

OFFICIAL BUSINESS

NO POSTAGE
NECESSARY
IF MAILED
IN THE
UNITED STATES

BUSINESS REPLY MAIL

FIRST CLASS PERMIT NO 0001,APG,MD

POSTAGE WILL BE PAID BY ADDRESSEE

DIRECTOR
US ARMY RESEARCH LABORATORY
ATTN AMSRL WM BD
ABERDEEN PROVING GROUND MD 21005-5066